A primordial origin for molecular oxygen in comets: a chemical kinetics study of the formation and survival of O_2 ice from clouds to discs

V. Taquet,[1][*] K. Furuya,[1] C. Walsh[1][*] and E. F. van Dishoeck[1,2][*]

[1]*Leiden Observatory, Leiden University, P.O. Box 9531, NL-2300 RA Leiden, the Netherlands*
[2]*Max-Planck-Institut für extraterretrische Physik, Giessenbachstrasse 1, D-85748 Garching, Germany*

ABSTRACT

Molecular oxygen has been confirmed as the fourth most abundant molecule in cometary material ($O_2/H_2O \sim 4$ per cent) and is thought to have a primordial nature, i.e. coming from the interstellar cloud from which our Solar system was formed. However, interstellar O_2 gas is notoriously difficult to detect and has only been observed in one potential precursor of a solar-like system. Here, the chemical and physical origin of O_2 in comets is investigated using sophisticated astrochemical models. Three origins are considered: (i) in dark clouds; (ii) during forming protostellar discs; and (iii) during luminosity outbursts in discs. The dark cloud models show that reproduction of the observed abundance of O_2 and related species in comet 67P/C-G requires a low H/O ratio facilitated by a high total density ($\geq 10^5$ cm^{-3}), and a moderate cosmic ray ionization rate ($\leq 10^{-16}$ s^{-1}) while a temperature of 20 K, slightly higher than the typical temperatures found in dark clouds, also enhances the production of O_2. Disc models show that O_2 can only be formed in the gas phase in intermediate disc layers, and cannot explain the strong correlation between O_2 and H_2O in comet 67P/C-G together with the weak correlation between other volatiles and H_2O. However, primordial O_2 ice can survive transport into the comet-forming regions of discs. Taken together, these models favour a dark cloud (or 'primordial') origin for O_2 in comets, albeit for dark clouds which are warmer and denser than those usually considered as Solar system progenitors.

Key words: astrochemistry – comets: individual: 67P/C-G – protoplanetary discs – stars: formation – ISM: abundances – ISM: molecules.

1 INTRODUCTION

Molecular oxygen, O_2, is a dominant component of Earth's atmosphere (21 per cent by volume). Because it is a by-product of photosynthesis (and also a reactant in cellular respiration), it is considered as a potential marker for biological activity on terrestrial-like exoplanets (e.g. Snellen et al. 2013). Atomic oxygen is the third most abundant element in the Universe (following H and He); however, it is still unknown what fraction of oxygen is contained within the deceptively simple O_2 in interstellar and circumstellar material.

Gas-phase O_2 has recently been observed in situ in the coma of comet 67P/Churyumov-Gerasimenko (hereafter comet 67P/C-G; Bieler et al. 2015) by the Rosetta Orbiter Spectrometer for Ion and Neutral Analysis (ROSINA) instrument on board the *Rosetta* spacecraft (Balsiger et al. 2007). O_2 is strongly correlated with H_2O and is present at an average level of 3.8 ± 0.85 per cent relative to H_2O, making it the fourth most abundant molecule in the

comet, following H_2O, CO_2, and CO. The authors argue that O_2 does not originate from gas-phase chemistry in the coma but from direct sublimation from or within the comet surface. The strong correlation with H_2O suggests that the O_2 is trapped within the bulk H_2O ice matrix of the comet, which provides constraints concerning the chemical origin of the O_2 ice. Processing of the cometary surface by solar wind particles and ultraviolet (UV) radiation has been ruled out by the authors, because the penetration depth (a few μm to m) is not sufficient to process material throughout the bulk. This process has been postulated to be responsible for the O_2-rich, yet tenuous, atmospheres of several of the icy moons of Saturn and Jupiter (e.g. Hall et al. 1995; Spencer, Calvin & Person 1995; Teolis et al. 2010). Upon each pass into the inner Solar system, comet 67P/C-G loses several metres of surface ice; hence, the surface revealed today is likely pristine. A reanalysis of data from the Neutral Mass Spectrometer on board the *Giotto* probe which did a fly-by of comet 1P/Halley in 1986, confirmed the presence of O_2 at a level similar to that seen in 67P/C-G (Rubin et al. 2015b). This suggests that O_2 is not only an abundant molecule in comets, but is also common to both Jupiter-family comets, such as 67P/C-G, and Oort Cloud comets, such as 1P/Halley, which have different dynamical behaviours and histories.

The 67P/C-G observations strongly suggest that O_2 was present within the ice mantle on dust grains in the pre-solar nebula prior to comet formation. This then raises the question whether O_2 was abundant in icy dust mantles entering the protoplanetary disc of the young Sun, or whether the conditions in the comet-forming zone of the early Solar system were favourable for O_2 formation and survival. Upper limits on the abundance of O_2 ice in molecular clouds obtained with the *Infrared Space Observatory* (*ISO*) and ground-based instruments are rather conservative ($O_2/H_2O < 0.6$; Vandenbussche et al. 1999; Pontoppidan et al. 2003). O_2 is a diatomic homonuclear molecule with zero electric dipole moment; hence it does not possess electric dipole-allowed rotational transitions which makes it difficult to detect in cold environments via remote sensing. Therefore, gas-phase O_2 has been particularly elusive in interstellar clouds, early attempts to detect gas-phase O_2 in molecular clouds with the *Submillimeter Wave Astronomy Satellite* (*SWAS*) and *Odin* resulted in upper limits only, $\lesssim 10^{-7}$ relative to H_2 (Goldsmith et al. 2000; Pagani et al. 2003).

More recent and higher sensitivity observations with *Herschel* allowed a deep search for O_2 towards sources considered true Solar system progenitors: low-mass protostars. A deep upper limit was determined towards the well-studied protostar, NGC 1333–IRAS 4A ($O_2/H_2 < 6 \times 10^{-9}$; Yildiz et al. 2013). Detailed modelling of the chemistry throughout the well-characterized envelope of IRAS 4A demonstrates that the material entering the protoplanetary disc, both gas and ice, is likely poor in molecular oxygen. For a H_2O/H_2 abundance of $\sim 5 \times 10^{-5}$, the inferred limit would correspond to a O_2/H_2O abundance ratio of ≤ 0.012 per cent. This picture is consistent with laboratory experiments that have shown that O_2 ice is efficiently hydrogenated at low temperatures and converted into H_2O and H_2O_2 ices ($\lesssim 30$ K; Ioppolo et al. 2008; Miyauchi et al. 2008). This makes the close association of O_2 with H_2O in 67P/C-G an even stronger enigma.

However, *Herschel* did reveal the presence of gas-phase O_2 in two sources: Orion ($O_2/H_2 \approx 0.3$–7.3×10^{-6}; Goldsmith et al. 2011; Chen et al. 2014) and ρ Oph A ($O_2/H_2 \approx 5 \times 10^{-8}$; Larsson et al. 2007; Liseau et al. 2012). Orion is a region of active star formation and the location of the gas-phase O_2 emission coincides with a clump of very warm (65–120 K) and dense gas, a so-called H_2 'hotspot', which may have recently been subjected to shocks (e.g. Melnick & Kaufman 2015). These conditions are not representative of those expected in the molecular cloud from which the Sun formed. On the other hand, ρ Oph A is a dense core in the more quiescent ρ Oph molecular cloud complex, which stands out from other low-mass star-forming regions by exhibiting emission from relatively warm molecular gas ($\gtrsim 20$ K; Liseau et al. 2010; Bergman et al. 2011a). Subsequent observations of ρ Oph A have also determined the presence of related gas-phase species, HO_2 and H_2O_2, at an abundance level on the order of 2×10^{-3} that of O_2 (Bergman et al. 2011b; Parise, Bergman & Du 2012). These molecular ratios show reasonable agreement with those seen in 67P/C-G with ROSINA ($HO_2/O_2 = (1.9 \pm 0.3) \times 10^{-3}$, $H_2O_2/O_2 = (0.6 \pm 0.07) \times 10^{-3}$; Bieler et al. 2015). The chemically related species, O_3 (ozone), was not detected in the comet coma with a very low upper limit, $< 2.5 \times 10^{-5}$ with respect to O_2.

In summary, despite O_2 being a particularly elusive molecule in interstellar and circumstellar environments, there apparently do exist conditions which are favourable for the formation of O_2 and related species at abundance ratios similar to that observed in ices in comet 67P/C-G. By assuming that all the energy deposited into water ice by high energy particles is used to convert H_2O into O_2, Mousis et al. (2016) claimed that radiolysis of water-containing interstellar ices in molecular clouds is the only mechanism that produces O_2 in high abundances. However, laboratory experiments of cold interstellar ice analogues show that O_2 can also be efficiently formed through non-energetic surface chemistry before being converted to water (see Minissale, Congiu & Dulieu 2014) while the production of O_2 through water radiolysis should be accompanied by a more efficient production of H_2O_2, in contradiction with the low abundance of H_2O_2 observed in 67P/C-G.

Here we investigate the formation and survival of O_2 ice using a variety of sophisticated astrochemical models, taking an extended chemical network including the formation and destruction pathways of O_2 into account, in order to elucidate the origin of cometary O_2, and help explain its strong correlation with water ice and the low abundances of its chemically related species. We explore and discuss several different origins: (i) O_2 synthesis in ice mantles in dark clouds ('primordial' origin); (ii) O_2 formation and survival en route from the protostellar envelope into the disc and subsequent delivery into the comet-forming zone; and (iii) in situ formation of O_2 within the protoplanetary disc prior to comet formation. This work differs from that presented in Mousis et al. (2016) because we consider all possible chemical pathways between O_2 and other O-bearing species, including H_2O, HO_2, H_2O_2, and O_3. In Section 2 we describe the interstellar chemistry of molecular oxygen, in Sections 3– 5 we systematically discuss each scenario, presenting the necessary evidence for or against each hypothesis, and in Section 6 we summarize our main findings.

2 INTERSTELLAR CHEMISTRY OF O_2

Two main processes have been invoked for the formation of molecular oxygen in the interstellar medium: (i) gas-phase formation via neutral–neutral chemistry, and (ii) formation via association reactions on/within icy mantles of dust grains. The observations towards both ρ Oph A and 67P/C-G, in conjunction with known chemical pathways studied in the laboratory, present several challenges for astrochemical models. First, the reproduction of the relatively high O_2/H_2O ice ratio simultaneously with the very low O_3/H_2O ice ratio, and second, the ratios of HO_2/O_2 and H_2O_2/O_2 produced in the gas phase, assuming that chemistry on or within the ice mantle is responsible for the observed gas-phase ratios. Fig. 1 summarizes the chemical reactions involved in the formation and destruction of molecular oxygen which are discussed here.

2.1 Gas-phase chemistry

Gaseous O_2 is thought to form primarily via the barrierless neutral–neutral reaction between O and OH in cold and warm gas. Because of its importance, this reaction has been well studied both experimentally and theoretically. The rate coefficient has a negligible temperature dependence, with a recommended value (based on theoretical calculations and experiments) between 2×10^{-11} and 8×10^{-11} cm^3 s^{-1} at 10 K, and an experimentally constrained value of 7×10^{-11} cm^3 s^{-1} at 140 K decreasing to 3×10^{-11} cm^3 s^{-1} at 300 K (see Hincelin et al. 2011, for a discussion on the rate coefficient). The formation of O_2 in cold dark clouds is initiated by the high initial abundance assumed for atomic oxygen, inducing an efficient ion–neutral chemistry that also forms OH. In warm environments ($T \gtrsim 100$ K), e.g. the inner regions of protostellar envelopes or the inner, warm layers of protoplanetary discs, OH and O are mostly produced through warm neutral–neutral chemistry driven by the photodissociation of water sublimated from interstellar ices. The gas-phase formation of the chemically related species,
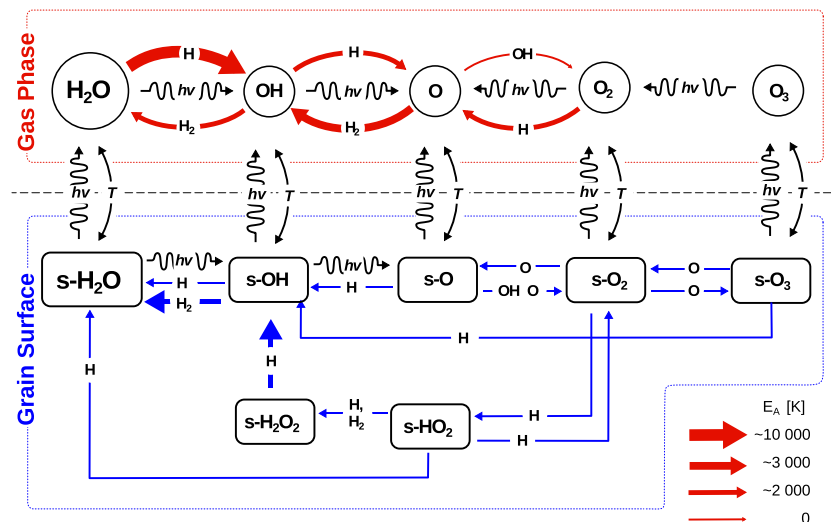
Figure 1. Summary of the main gas-phase and solid-state chemical reactions leading to the formation and the destruction of molecular oxygen. Gas-phase neutral–neutral reactions have activation barriers whose values are estimated by the thickness of the arrow. s-X denote species X on the ice surfaces.

O_3, is inefficient under interstellar conditions, as it requires three-body association of $O_2 + O$ (Atkinson et al. 2004); thus, despite this reaction possessing a negligible reaction barrier, it only proceeds under the high-density conditions found in planetary atmospheres and in the inner midplanes of protoplanetary discs.

2.2 Ice chemistry

Solid O_2 in dark clouds is involved in the surface chemistry reaction network leading to the formation of water ice (Tielens & Hagen 1982; Cuppen et al. 2010; van Dishoeck, Herbst & Neufeld 2013). O_2 is formed through atomic O recombination on ices and efficiently reacts with either atomic O or atomic H to form O_3 or HO_2, respectively, eventually leading to the formation of water. The hydrogenation of O_3 also leads to the formation of O_2, in addition to dominating the destruction of O_3 ice.

Laboratory experiments of interstellar ice analogues studying water formation suggest that the O + O, O + O_2, and H + O_2 reactions, involved in the formation and destruction of O_2, all have small or negligible reaction barriers. Miyauchi et al. (2008) and Ioppolo et al. (2008) independently studied the efficiency of the O_2 + H reaction, with both studies concluding that this reaction is effectively barrierless, contradicting the earlier quantum calculations by Melius & Blint (1979) for the gas-phase reaction which predicted an activation barrier of 1200 K. The reactivity of the O + O and O + O_2 reactions is still a matter of debate, and is discussed in Section 2.4. The reaction, $O_3 + O \longrightarrow O_2 + O_2$, is considered unlikely to occur on grain surfaces under dark cloud conditions because of its relatively high activation energy barrier, 2000 K, as experimentally determined for the gas-phase reaction (Atkinson et al. 2004).

Dark clouds, the inner regions of protostellar envelopes, and the comet-forming regions of protoplanetary discs, are all well-shielded from external sources of UV radiation ($A_V \gtrsim 10$ mag); however, water ice can be photodissociated by cosmic ray-induced UV photons produced by the excitation of molecular hydrogen by electrons generated by cosmic ray ionization of H_2 (Prasad & Tarafdar 1983). Water ice photodissociation has been extensively studied in the lab-

oratory (Westley et al. 1995; Öberg et al. 2009) and in molecular dynamics (MD) simulations (Andersson et al. 2006; Andersson & van Dishoeck 2008; Arasa et al. 2015). The MD simulations show that water ice which is photodissociated generates OH and H photoproducts that move through the ice due to their excess energy. Each photodissociation event can lead to various chemical outcomes (e.g. direct desorption into the gas phase or recombination followed by desorption or trapping), the probabilities for which are dependent upon the depth into the ice mantle (and fully tabulated in Arasa et al. 2015). The detection of O_2 following the UV irradiation of cold water ice also supports water ice photodissociation into O + H_2 or O + H + H photoproducts (Öberg et al. 2009; Heays, Bosman & van Dishoeck 2016).

Laboratory experiments show that the bombardment of cold water ices with ionizing energetic particles can result in the formation of O_2 and other chemically related species from the destruction of water (see Matich et al. 1993; Sieger, Simpson & Orlando 1998; Baragiola et al. 2002; Loeffler et al. 2006; Zheng, Jewitt & Kaiser 2006; Teolis et al. 2010; Hand & Carlson 2011). The production of O_2 and H_2O_2 through irradiation of water ice by energetic particles depends on the projectile penetration depth. Low-energy ions, for example, only penetrate the few dozen outermost ice layers, where H and H_2 can easily escape, favouring an efficient production of O_2 relative to H_2O_2. The yield of O_2 production therefore tends to decrease with the energy of the irradiating particles from a few 10^{-3} molecule eV^{-1} for keV protons to 10^{-6} for MeV ions (see Teolis et al. 2010). Irradiation of energetic ions during the condensation of water molecules can dramatically enhance the production of O_2 up to O_2/H_2O abundances ratios of ~30 per cent (Teolis et al. 2006).

2.3 Gas–ice balance

O_2 formed in the ice mantle under dark cloud conditions ($T \sim 10$ K) can be returned to the gas phase via a multitude of non-thermal desorption processes (e.g. Tielens 2013). Those mechanisms which have been quantified in the laboratory for O_2 include photodesorption by cosmic ray-induced UV photons (Fayolle et al.

2013; Zhen & Linnartz 2014), and desorption induced by exothermic chemical reactions (i.e. chemical desorption; Minissale & Dulieu 2014; Minissale et al. 2016). Photodesorption of O_2 was found to be triggered by photodissociation, with O_2 returned to the gas phase with yields of $\sim 10^{-3}$ molecules per incident photon, for a radiation spectrum appropriate for the cosmic ray-induced UV field and pure O_2 ice (Fayolle et al. 2013). O_3 is also detected in the experiments by Zhen & Linnartz (2014) with yields a factor of a few lower than those for O_2. O_3 is not seen in the experiments by Fayolle et al. (2013) due to the lower FUV fluences in the synchrotron experiments.

The probability of chemical desorption depends strongly on the type of reaction and on the substrate and can vary between 0 and 80 per cent. The chemical desorption efficiency of the O + O reaction was found to be ≈ 80 per cent in experiments of O_2 formation via oxygen recombination on bare olivine-type surfaces (Minissale & Dulieu 2014). However, in experiments with higher oxygen coverage, the efficiency was reduced to an estimated upper limit of ≈ 5 per cent probably due to an efficient dissipation of the energy released by the exothermic reaction into the water ice (Minissale & Dulieu 2014; Minissale et al. 2016). The standard chemical desorption efficiencies assumed in this work are the theoretical values computed by Minissale et al. (2016) for the submonolayer regime on bare grains. However, they should be regarded as upper limits. The O + O reaction has a high theoretical probability of 68 per cent while reactions O_2 + H, HO_2 + H, and H_2O_2 + H show much lower theoretical chemical desorption probabilities of 0.5–2 per cent, in agreement with the experimental upper limits. We explore in Section 3.2 the impact of the chemical desorption efficiencies on the gas-phase abundances of O_2 and its chemically related species. When data are not available, the chemical desorption probability is fixed to 1.2 per cent (Garrod, Wakelam & Herbst 2007).

The binding energies of O_2 to a variety of surfaces, including dust-grain analogues and water ice, have been measured in the laboratory (≈ 900 K; Collings et al. 2004, 2015; Fuchs et al. 2006; Acharyya et al. 2007; Noble et al. 2012). This low binding energy makes O_2 a particularly volatile species, expected to desorb at temperatures similar to CO. In temperature-programmed desorption (TPD) experiments with O_2 layered on top of, and fully mixed with, water ice, a fraction of O_2 is found to remain trapped within the ice matrix and released at higher temperatures (Collings et al. 2004). The trapped fraction depends upon the deposition temperature with a greater fraction of volatiles trapped within the water ice when deposited at lower temperatures (Collings et al. 2003).

2.4 Important parameters for the chemistry of O_2

The O_2 formation and survival in dark clouds and protoplanetary discs depends on a number of parameters, which are linked in turn to various physical and chemical conditions.

(1) The gas-phase abundance ratio between H and O atoms that accrete on to grains governs the competition between hydrogenation reactions leading to H_2O_2 and H_2O and association reactions between O atoms, forming O_2 or O_3 (Tielens & Hagen 1982). For dark cloud conditions, the atomic H abundance in the gas phase is a balance between its formation, which occurs via H_2 ionization followed by dissociative electron recombination, and its conversion back into H_2 via recombination reactions on grain surfaces. At steady state and assuming a sticking probability of 1, the density

of H is therefore given by the ratio between these two processes (Tielens 2005):

$$n(H) = \frac{2.3 \zeta n(H_2)}{2 v(H) \sigma_d X_d n(H_2)}, \qquad (1)$$

where $v(H)$ is the thermal velocity of atomic hydrogen, ζ the cosmic ray ionization rate, and X_d and σ_d the abundance and the cross-section of interstellar grains. The absolute number density of atomic H is therefore independent of the total density and increases linearly with the cosmic ray ionization rate. Since the initial number density of atomic O increases linearly with the total number density for a fixed oxygen abundance, the atomic H/O abundance ratio increases (decreases) linearly with the total density (cosmic ray ionization rate).

(2) The surface mobility of O atoms governs the reactivity of the O + O and O + O_2 reactions. The surface mobility of O atoms occurs mostly through thermal hopping and depends exponentially on the dust temperature T, and their diffusion energy E_d. Astrochemical models which treat grain-surface chemistry usually scale the diffusion energy to the binding energy of the considered species $E_b(i)$, using a fixed value for the diffusion-to-binding energy ratio E_d/E_b (e.g. Tielens & Allamandola 1987). As discussed by several authors (Cuppen & Herbst 2007; Taquet, Ceccarelli & Kahane 2012), E_b and E_d/E_b strongly depend upon the ice morphology and composition. The mobility of atomic oxygen on interstellar ice analogues has recently been investigated by several experimental groups (Bergeron et al. 2008; He et al. 2015) who conclude that atomic O has a higher binding energy than the value of 800 K estimated by Tielens & Allamandola (1987). Theoretical calculations and experiments studying the diffusion of molecules (CO or CO_2) or heavy atoms (O) on several types of substrates suggest that species diffuse with low diffusion-to-binding energy ratios of the order of 30–50 per cent (Jaycock & Parfitt 1986; Karssemeijer & Cuppen 2014). However, experiments focusing on H_2 formation via H recombination on surfaces suggest a higher diffusion-to-binding energy ratio between 50 and 80 per cent (Katz et al. 1999; Perets et al. 2005; Matar et al. 2008). The diffusion-to-binding energy ratio likely has a distribution of values that depend upon the substrate (bare or ice-coated), the species under consideration (light atom, heavy atom, molecule), the ice morphology (porous, compact, crystalline, or amorphous ice), and the dominant composition of the chemically active surface layer (H_2O, CO_2, or CO).

(3) The activation barriers of the O + O and O + O_2 reactions directly govern the reactivity of the two reactions. Minissale et al. (2014) derive an upper limit of 150 K for the reaction barrier for O + O and O + O_2 in an experimental study on an amorphous silicate surface. However, the presence of an activation barrier for the latter reaction has been invoked by several authors (see Dulieu 2011). For example, Lamberts et al. (2013) require an activation barrier of 500 K for the O + O_2 reaction in order to reproduce the results of laboratory experiments in thick ices with their microscopic Monte Carlo model. Here we explore the effects of the parameter choices for these three key aspects of the O_2 chemistry.

2.5 Astrochemical models

Three state-of-the-art gas-grain astrochemical models have been used in this work to study the formation and survival of molecular oxygen from dark clouds to the Solar system: (1) the multiphase model by Taquet, Charnley & Sipilä (2014) to study the formation of O_2 in dark clouds; (2) the multiphase model by Furuya et al. (2015) to study the formation of O_2 during the formation of protoplanetary

discs; (3) the two-phase model by Walsh, Nomura & van Dishoeck (2015) to study the formation of O$_2$ in situ in protoplanetary discs.

The multiphase gas-grain Taquet and Furuya models couple the gas-phase and ice chemistries with the approach developed by Hasegawa & Herbst (1993) to follow the multilayer formation of interstellar ices and to determine the gas–ice balance. Several sets of differential equations governing the time evolution of abundances are considered: one for gas-phase species, one for surface ice-mantle species, and one (or several) for bulk ice-mantle species. The equations governing chemical abundances on the ice surface and in the bulk ice are linked by an additional term that is proportional to the rate of growth or loss of the grain mantle. As a consequence, surface species are continuously trapped in the bulk because of the accretion of new species in dark clouds. Following Vasyunin & Herbst (2013), the chemically active surface is limited to the top four monolayers. The bulk ice mantle is considered to be chemically inert. The original three-phase model considered in the Taquet model assumes that the inert bulk ice mantle has a uniform molecular composition. In order to accurately follow the ice evolution in warm conditions, the Furuya model considers a depth-dependent molecular composition, through the division of the inert bulk ice mantle into five distinct phases (for details, see Furuya et al. 2016, and references therein).

Radiolysis, i.e. the bombardment of (ionizing) energetic particles depositing energy into the ice, and/or photolysis, i.e. the irradiation of ultraviolet photons breaking bonds, can trigger chemistry within the bulk mantle of cold interstellar ices. We have investigated the impact of the UV photolysis induced by secondary UV photons on the bulk ice chemistry and the formation and survival of O$_2$ by activating the bulk chemistry and assuming the same ice parameters as for the surface chemistry (same diffusion and binding energies, same chemical reactions). In our model, the formation of O$_2$ from H$_2$O photodissociation is a multistep process, starting from the production of oxygen atoms from water or OH photodissociation followed by their recombination. We find that O$_2$ cannot be efficiently produced in the bulk through ice photolysis as the photodissocation of the main ice components not only produces oxygen atoms, that recombine together to form O$_2$, but also hydrogen atoms that react with O$_2$ to reform water even if H$_2$O ice photodissociation would go directly to H$_2$ rather than H since there are other molecules like CH$_4$, NH$_3$, or CH$_3$OH that produce hydrogen atoms that are very mobile. Overall, activating the bulk chemistry decreases the abundance of highly reactive species like O atoms or radicals but does not affect the main ice species.

Laboratory experiments show that O$_2$ can be efficiently formed through radiolysis of ices without overproducing H$_2$O$_2$ only if the radiolysis occurs as water is condensing on to a surface (Teolis et al. 2006, see Section 2.2). However, in molecular clouds water ice is mostly formed in situ at the surface of interstellar grains through surface reactions involving hydrogen and oxygen atoms. This happens prior to the formation of the pre-solar nebula, i.e. the cloud out of which our Solar system was formed, and it is possible that the comet-forming zone of the Sun's protoplanetary disc inherited much of its water ice from the interstellar phase (Visser et al. 2009; Cleeves et al. 2014; Altwegg et al. 2015; Furuya et al. 2016). For the radiolysis mechanism to occur in the pre-solar nebula, water ice would first need to be completely sublimated and then recondensed prior to comet formation. Luminosity outbursts induced by instabilities in the disc of the solar nebula can potentially provide a scenario for efficient O$_2$ production in the ice matrix through sudden evaporation of water ice followed by fast recondensation. We consider this scenario less likely because the cosmic ray ionization rate is thought to be impeded near the disc midplane with respect to

interstellar values (e.g. Cleeves, Adams & Bergin 2013). Energetic ionizing particles from the (pre)solar wind are also expected to be significantly attenuated close to the disc midplane by the intervening large column of material ($\gg$100 g cm^{-2}) between the central star and the comet-forming zone beyond $\sim$10 au.

Mousis et al. (2016) explored the O$_2$ formation through radiolysis of water within interstellar ices in the solar nebula to explain the high abundance of O$_2$ observed in comet 67P/C-G. However, they concluded that the galactic cosmic ray flux is not sufficient to produce the observed ratio of O$_2$/H$_2$O over the lifetime of the pre-solar nebula.

The gas-phase chemical network used by the Taquet model is the non-deuterated version of that from Taquet et al. (2014), the basis for which is the 2013 version of the Kinetic Database for Astrochemistry (KIDA) chemical data base (Wakelam et al. 2012). It has been further updated to include warm gas-phase chemistry involving water and ion-neutral reactions involving ozone. The network also includes the surface chemistry of all dominant ice components (H$_2$O, CO, CO$_2$, NH$_3$, CH$_4$, H$_2$CO, CH$_3$OH), as well as those important for water (e.g. O$_2$, O$_3$, and H$_2$O$_2$). Several new surface reactions were added involving O$_3$ and reactive species such as N, O, OH, NH$_2$, and CH$_3$, following the NIST gas-phase chemical data base.

The gas–ice chemical network of Garrod & Herbst (2006), based on the OSU 2006 network, is used with the Furuya model. The gas phase and surface networks are more suited to the high density and warm temperatures conditions found in protostellar envelopes. It has therefore been supplemented with high-temperature gas-phase reactions from Harada, Herbst & Wakelam (2010) and includes the formation of many complex organic molecules. It is consequently more expansive than the network used in the Taquet model.

The gas-phase chemical used in the Walsh model is based on the 2012 release of the UMIST Database for Astrochemistry (UDfA; McElroy et al. 2013), supplemented by direct X-ray ionization reactions, X-ray-induced ionization and dissociation processes, and three-body reactions. The grain surface chemical network of Garrod, Weaver & Herbst (2008) is used.

Input parameters assumed for the three types of astrochemical models are listed in Table 1. Unless otherwise stated, this table gives the standard values for the physical parameters: the cosmic ray ionization rate ζ, the flux of secondary UV photons; the grain surface parameters: the dust-to-gas mass ratio R_{dg}, the grain diameter a_s, the volumic mass of grains ρ_d, the surface density N_s, the diffusion-to-binding energy ratio E_d/E_b, the number of chemically active monolayers N_{act}, and the sticking coefficient of species heavier than H and H$_2$. The elemental abundances of species correspond to the set EA1 from Wakelam & Herbst (2008).

3 DARK CLOUD ORIGIN?

Here we investigate whether the O$_2$ observed in 67P/C-G has a dark cloud origin, using the chemistry of O$_2$ ice and gas described in the previous section. For this purpose, we use the Taquet astrochemical model presented in Section 2.4. Appendix A presents a first parameter study, in which several surface and chemical parameters are varied, in order to reproduce the low abundances of the chemically related species O$_3$, HO$_2$, and H$_2$O$_2$ with respect to O$_2$ seen in comet 67P/C-G. The low abundance of O$_3$ and HO$_2$ relative to O$_2$ can be explained when a small activation barrier of $\sim$300 K is introduced for the reactions O + O$_2$ and H + O$_2$, in agreement with the Monte Carlo modelling of Lamberts et al. (2013). However, the abundance of H$_2$O$_2$ is still overproduced by one order of magnitude,

Table 1. Input parameters assumed in all simulations.

Input parameters	Values
Standard physical parameters	
ζ (s^{-1})	10^{-17}
F(sec. UV) (cm^{-2} s^{-1})	10^4
Grain surface parameters	
R_{dg}	0.01
a_d (μm)	0.2
ρ_d (g cm^{-3})	3
N_s (cm^{-2})	10^{15}
E_d/E_b	0.5
N_{act} (MLs)	4
S (heavy species)	1
Initial abundances	
$X(H_2)$	0.5
$X(He)$	0.09
$X(C)$	7.30×10^{-5}
$X(N)$	2.14×10^{-5}
$X(O)$	1.76×10^{-4}
$X(Si)$	8.0×10^{-9}
$X(S)$	8.0×10^{-8}
$X(Fe)$	3.0×10^{-9}
$X(Na)$	2.0×10^{-9}
$X(Mg)$	7.0×10^{-9}
$X(Cl)$	1.0×10^{-9}

suggesting that other chemical processes might be at work. A second parameter-space study is then conducted to determine the range of physical conditions (e.g. dust temperature, number density, and cosmic ray ionization rate) over which O_2 ice and gas (and those for chemically related species, O_3, HO_2, and H_2O_2) reach abundances (relative to water ice) similar to that seen in 67P/C-G. Finally, the case of ρ Oph A, where gas-phase O_2 has been detected in the gas phase, is revisited with the same chemical model.

3.1 Impact of physical and chemical parameters

The low temperature, in conjunction with the low flux of UV photons found in interstellar dark clouds, promotes the formation of interstellar ices. The ice chemical composition depends on various physical and chemical parameters as discussed in Section 2.4. To investigate the formation and survival of O_2 under dark cloud conditions, a model grid is run in which the total density of H nuclei, n_H, the gas and dust temperature, T (assumed to be equal), the cos-

mic ray ionization rate, ζ, and the visual extinction, A_V, are varied following the methodology described in Taquet et al. (2012). Values explored in the model grid are listed in Table 2, resulting in 500 models in total. In these models, the 'standard' set of chemical parameters derived in Appendix A are assumed (see Table 2).

The abundances of all species in the reaction network are evolved from their assumed initial abundances (see Section 2.5) as a function of time only, i.e. assuming constant physical conditions. Fig. 2 shows the distribution of abundances of solid O_2, and the chemically related species, O_3, HO_2, and H_2O_2, relative to water ice, at the free-fall time, t_{FF}, defined as

$$t_{FF} = \sqrt{\frac{3\pi}{32\, G n_H m_p}}\; \text{s},\qquad(2)$$

where G is the gravitational constant and m_p is the proton mass. t_{FF} varies across the grid from 4.4×10^4 to 1.4×10^6 yr. Cores can have longer lifetimes, e.g. due to magnetic support, up to $10\, t_{FF}$. However, assuming a longer time-scale does not change our conclusions because interstellar ices form in a time-scale similar to t_{FF}. The results show that the formation and survival of solid O_2, and other reactive species, in interstellar ices, is strongly dependent upon the assumed physical conditions. The model grid shows a large dispersion of final abundances of solid O_2 from $<10^{-10}$ to 10 relative to water ice (top panel of Fig. 2). Because of its lower reactivity, hydrogen peroxide, H_2O_2, shows a slightly more narrow final abundance dispersion, with most of the models predicting values between 10^{-6} and 10^{-2} (1 per cent) with respect to water ice (see bottom panel of Fig. 2). HO_2 is mostly formed in the ice mantle via the hydrogenation of O_2, and is converted into H_2O_2 via a subsequent barrierless hydrogenation reaction, O_2 being a precursor of H_2O_2; hence, its final abundance is governed by that of O_2 ice, and therefore follows a similar trend but lower by four orders of magnitude due its high reactivity. Ozone formed from molecular oxygen via the $O_2 + O$ reaction also displays a broad distribution of abundances but most of the models predict abundances lower than 10^{-6} relative to water, due to the small $O + O_2$ barrier.

Fig. 3 shows the distribution of the final abundance of solid O_2 relative to water ice, for the range of assumed values for each physical parameter varied in the model grid. High O_2 abundances (>4 per cent relative to water ice) are obtained only for those models with high densities ($n_H \gtrsim 10^5$ cm^{-3}). As discussed in Section 2.4, higher gas densities result in a lower gas-phase H/O ratio, thereby increasing the rate of the association reaction between O atoms to form O_2 ice, and correspondingly decreasing the rate of the hydrogenation reactions, $O + H$ and $O_2 + H$, which compete with O_2 ice formation, and destroy O_2 ice once formed, respectively.

Table 2. Physical conditions and their range of values explored in the model grid.

Parameter	Range of explored values	Standard value
Total density n_H (cm^{-3})	10^3–10^4–10^5–10^6	10^6
Temperature $T_{gas} = T_{dust}$ (K)	10–15–20–25–30	21
Cosmic ray ionization rate ζ (s^{-1})	10^{-18}–3×10^{-18}–10^{-17}–3×10^{-17}–10^{-16}	10^{-17}
Visual extinction A_V (mag)	2–4–6–8–10	10
Chemical parameters explored individually in Appendix A		
E_d/E_b	0.3–0.8	0.5
$E_b(O)$ (K)	800–1700	1700
$E_a(O + O_2)$ (K)	0–300	300
$E_a(H + O_2)$ (K)	0–1200	300
$E_a(H + H_2O_2)$ (K)	0–2500	800

hand, the visual extinction does not have a strong impact on the abundance of solid O$_2$ as the distributions of abundances obtained for the five visual extinction values are very similar. Thus, the final O$_2$ ice abundances depend more strongly upon the assumed gas density, temperature, and cosmic ray ionization rate, and high O$_2$ ice abundances occur when the initial atomic H/O ratio is low ($\lesssim 10^{-2}$).

To illustrate further the crucial impact of the density and the cosmic ray ionization rate on the chemical composition of ices, Fig. 4 shows the evolution of the abundances of O$_2$ and its chemically related species with respect to water ice as a function of the initial atomic H/O abundance ratio induced by a variation of the total density (assuming a constant ζ of 10^{-17} s^{-1}) or a variation of the cosmic ray ionization rate (assuming $n_H = 10^6$ cm^{-3}) at $T = 10$ and 20 K. According to equation (1), the initial atomic H/O abundance ratio follows the expression

$$\left(\frac{H}{O}\right)_{ini} = 3.4 \times 10^{-3} \frac{\zeta}{10^{-17}\,\text{s}^{-1}} \frac{10^6\,\text{cm}^{-3}}{n_H} \frac{1.76 \times 10^{-4}}{X(O_{ini})} \sqrt{\frac{10\,\text{K}}{T}}$$

$$(3)$$

assuming the grain parameter values listed in Table 1. For each temperature case, the evolution of the abundance ratios with the initial atomic H/O abundance ratio follows similar trends, suggesting that the initial atomic H/O abundance ratio, and consequently the n_H/ζ ratio, is the dominant parameter for the formation and survival of O$_2$ and its chemically related species in dark clouds. The formation of O$_2$ ice is strongly inhibited (O$_2$/H$_2$O $\lesssim 1$ per cent) for high initial H abundances ([H]/[O]$_{ini} \gtrsim 5 \times 10^{-2}$) induced by high cosmic ray ionization rates and/or low densities, as it increases the rate of conversion of O$_2$ ice to H$_2$O ice. For low cosmic ray ionization rates or high densities inducing initial H/O ratios lower than 10^{-2}, the formation of H atoms in the gas phase is no longer dominated by H$_2$ ionization followed by dissociative recombination but by neutral–neutral reactions involving O atoms. The abundances of O$_2$ and other chemically related species are consequently no longer influenced by ζ nor n_H and remain constant. The results here demonstrate that a high abundance of O$_2$, at a level similar to that measured in 67P/C-G, seems to require an initial H/O abundance ratio lower than ~ 2–3×10^{-2} (depending on the temperature) or, according to equation (3)

$$\frac{n_H}{\zeta} \geq 10^{22}\,\text{cm}^{-3}\,\text{s}$$

$$(4)$$

assuming the initial abundances listed in Table 1.

Fig. 5 shows the chemical composition of the ice obtained for the model using the physical conditions that best reproduce the observations in comet 67P/C-G ($n_H = 10^6$ cm^{-3}, $T = 21$ K, $\zeta = 10^{-16}$ s^{-1}), and the chemical parameters derived in Appendix A. The fractional composition in each ice monolayer is plotted as function of monolayer number, i.e. the ice thickness that grows with time. At such a high density (10^6 cm^{-3}), hydrogenation reactions are less efficient due to the lower relative abundance of atomic H, and the freeze-out time-scales are sufficiently fast that reactive species can be trapped in the ice mantle before conversion into more stable molecules, like H$_2$O. The higher temperature (21 K) also enhances the mobility of heavier species, such O, to increase the relative abundance of ice species such as O$_2$ and CO$_2$. As a consequence, the most abundant species are water and carbon dioxide. O$_2$ ice is mostly present in the innermost layers of the ice mantle and decreases in relative abundance towards the ice surface, reflecting the initial low ratio of H/O in the gas phase, but tends to be well mixed with H$_2$O ice. In contrast, CO is mostly formed in the outer part of the ices, allowing
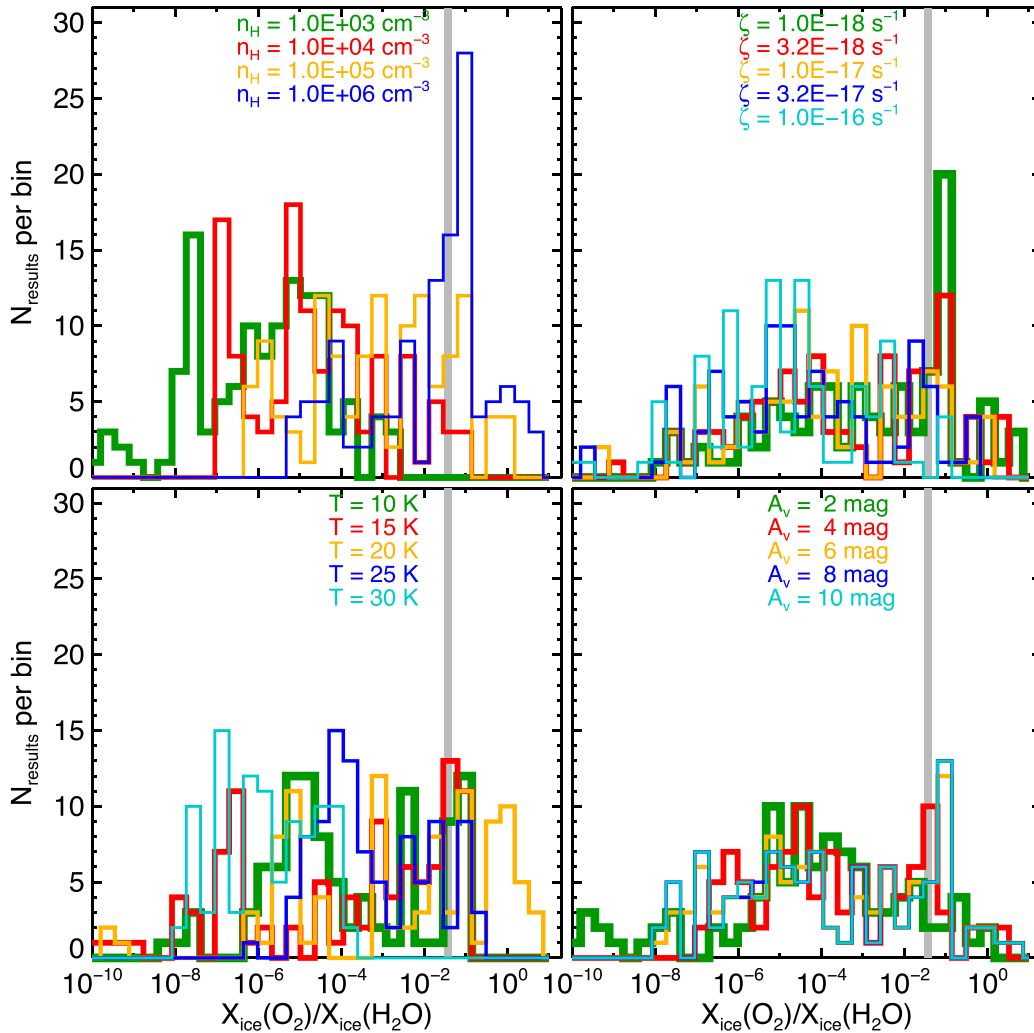

Figure 2. Distribution of final abundances of solid O$_2$ (green, top panel), O$_3$ (red), HO$_2$ (yellow), and H$_2$O$_2$ (blue, bottom panel) relative to water ice at the free-fall time (defined in the text), for the complete model grid in which the total density, the temperature, the cosmic ray ionization rate, and the visual extinction are varied within the range of values given in Table 2 (see Section 3.1). The thick dashed lines or the solid boxes refer to the abundances observed in the comet 67P/C-G.

An intermediate temperature of 20 K is also favoured because it enhances the mobility of oxygen atoms on the grain surfaces whilst at the same time allowing efficient sublimation of atomic H. This additionally enhances the rate of oxygen recombination forming O$_2$, with respect to the competing hydrogenation reactions. Models with lower temperatures of 10 or 15 K can also reproduce the O$_2$/H$_2$O of 4 per cent if a high density of $n_H \sim 10^6$ cm^{-3} is considered. Moreover, because the density of gas-phase H atoms increases linearly with the cosmic ray ionization rate, ζ, a low value of ζ also tends to favour the survival of O$_2$ ice. On the other

Figure 3. Distribution of final abundances of solid O_2 relative to water ice at the free-fall time (defined in the text), for the range of densities (top left), temperatures (bottom left), cosmic ray ionization rates (top right), and visual extinctions (bottom right), assumed in the model grid (see Section 3.1). For each panel, the 'standard' values of other parameters, listed in Table 2, are assumed. The grey solid boxes refer to the O_2 abundance observed in the comet 67P/C-G.

an efficient sublimation, explaining its weak correlation with water in 67P/C-G.

3.2 The ρ Oph A case

The ρ Oph A core, located at a distance of 120 pc, constitutes the best test case for the water surface network and the production of O_2 in dark clouds because it is the only interstellar source so far where gas-phase O_2, HO_2, and H_2O_2 have been detected (Bergman et al. 2011b; Liseau et al. 2012; Parise et al. 2012). The parameter study presented in the previous section suggests that the physical conditions of ρ Oph A, a high density ($n_H \sim 10^6$ cm^{-3}), and a relatively warm gas temperature ($T_{kin} = 24$–30 K) and dust temperature ($T_{dust} \sim 20$ K), derived by Bergman et al. (2011a) are consistent with those which facilitate the formation and survival of O_2 ice.

O_2, O_3, HO_2, and H_2O_2 are mostly, and potentially only, produced via surface chemistry; hence their gas-phase abundances depend on their formation efficiency in interstellar ices and on the probability of desorption upon formation through chemical desorption (which is the dominant non-thermal desorption mechanism for these species in dark cloud conditions). As explained in Section 2.3, the chemical desorption probabilities assumed in this work are the theoretical

values computed by Minissale et al. (2016) and Cazaux et al. (2016) for more than 20 reactions involved in the water and methanol chemical networks and vary between 0 and 70 per cent. When data are not available, the chemical desorption probability is fixed to 1.2 per cent (Garrod et al. 2007).

Fig. 6 shows the temporal evolution of the gas-phase abundances of O_2, O_3, HO_2, and H_2O_2 when the theoretical chemical desorption probabilities from Minissale et al. (2016), considered as our standard values, are assumed. The high chemical desorption probability of the reaction O + O (68 per cent) allows for an efficient evaporation of O_2 in the gas phase upon formation on ices, inducing maximal abundances of a few 10^{-6} obtained at 8000 yr. At longer time-scales, the O_2 production on ices is limited and the gas-phase abundance of O_2 decreases sharply in a few 10^4 yr due to its efficient freeze-out induced at the high density $n_H = 10^6$ cm^{-3}. The surface reactions O_2 + H and HO_2 + H forming HO_2 and H_2O_2 have a lower chemical desorption probability of 1.4 and 0.5 per cent, respectively. These values are nevertheless high enough to produce gaseous abundances of HO_2 and H_2O_2 larger than 10^{-8}. As a consequence, the model fails to simultaneously reproduce the gaseous abundances of O_2, HO_2, and H_2O_2 derived in ρ Oph A since the predicted HO_2 and H_2O_2 abundances are higher than the

Figure 5. Fractional composition of each ice monolayer as function of the monolayer number or ice thickness for the model that best reproduces the observations of comet 67P/C-G.
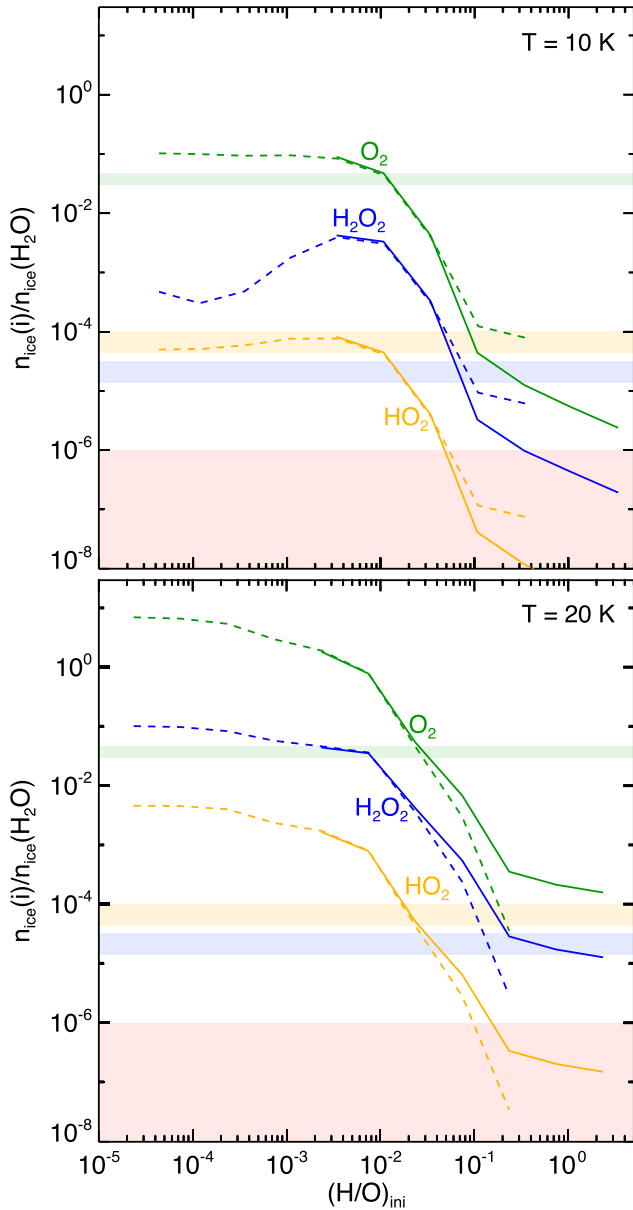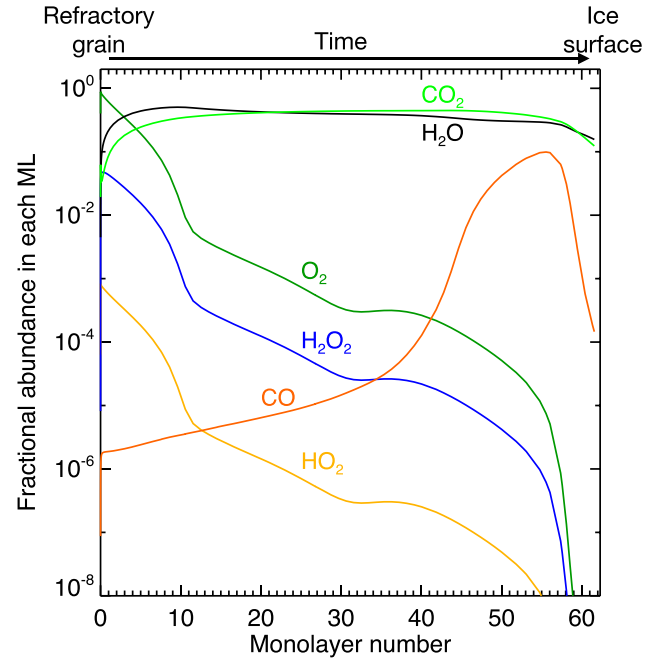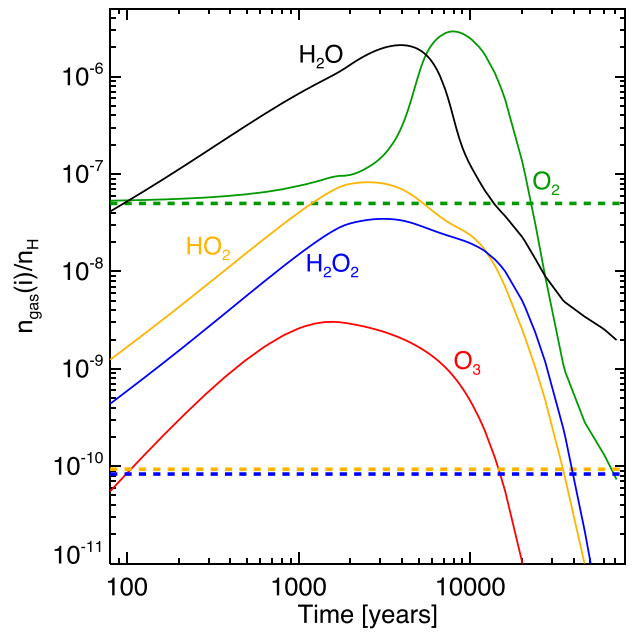

Figure 4. Final abundances of O_2, O_3, HO_2, and H_2O_2 in interstellar ices with respect to water as function of the initial H/O abundance ratios given by different cosmic ray ionization rates (and assuming $n_H = 10^6$ cm^{-3}, dashed lines) and different densities (and assuming $\zeta = 10^{-17}$ s^{-1}, solid lines) at $T = 10$ K (top) and $T = 20$ K (bottom). The 'standard' values of other parameters, listed in Table 2, are assumed. The solid boxes refer to the abundances observed in comet 67P/C-G.

Figure 6. Gas-phase abundances of O_2 and its chemically related species as a function of time predicted by the model using the ρ Oph A physical conditions and the chemical parameters derived in Appendix A.

observations by one order of magnitude when the predicted O_2 abundance reaches the observed value of 5×10^{-8} at a time of 1.8×10^4 yr. Instead, their abundances are fit at a slightly longer time of 3×10^4 yr.

Du & Parise (2012) also performed a comprehensive modelling of the gas–ice chemistry occurring for the physical conditions found in ρ Oph A by focusing on HO_2 and H_2O_2. Their chemical network is similar to that used in this work but they used a two-phase model where the entire bulk ice is assumed to be chemically reactive, and adopted a high chemical desorption probability of 10 per cent for all surface reactions. Their model therefore predicts a high abundance of gaseous HO_2 and H_2O_2, typically higher than 10^{-8} for the

first 10^5 yr of their simulation, and finds good agreement with the observations, with abundances of $\sim 10^{-10}$, at $t = 6 \times 10^5$, which is 10 times longer than the free-fall time-scale expected at this density. At this time-scale, the predicted O_2 abundance is one order of magnitude lower than the observed value of 5×10^{-8}, a similar result as our standard model. Fig. 7 shows the gas-phase abundances of HO_2, H_2O_2, and O_3 obtained when the predicted abundance of O_2 reaches the abundance observed towards ρ Oph A by decreasing the chemical desorption probability of all reactions with respect to their standard theoretical value. The model using a normalized
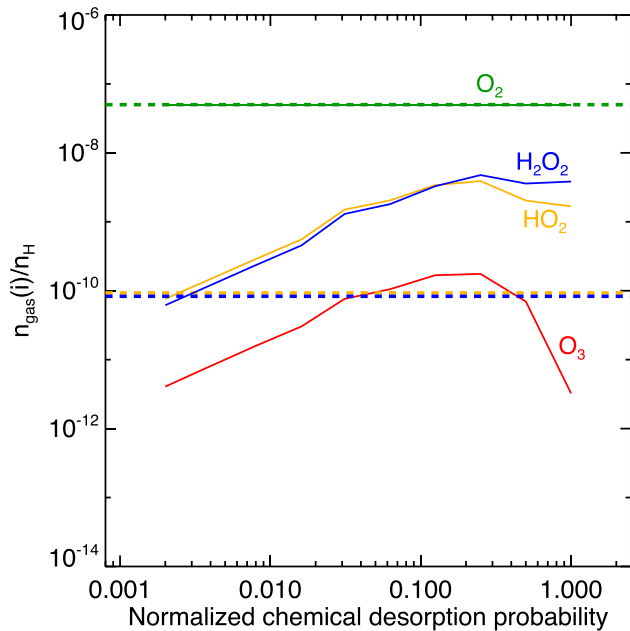
Figure 7. Gas-phase abundances of HO₂, H₂O₂, and O₃ obtained when the predicted abundance of O₂ reaches the abundance observed at $t = 4 \times 10^4$ yr towards ρ Oph A when decreasing the chemical desorption probability of all reactions with respect to their standard theoretical value.

chemical desorption probability of 1 is the standard model. It can be seen that the O₂, HO₂, and H₂O₂ abundances can be simultaneously reproduced when chemical desorption probabilities lower than the standard values by a factor of 500 are used, giving absolute values of ~0.001 per cent for the reactions H + O₂ and H + HO₂.

4 PROTOSTELLAR OR DISC FORMATION ORIGIN?

The models presented and discussed in the preceding section show that O₂ (and chemically related species) can be efficiently formed under dark cloud conditions, reaching abundance levels (relative to water ice) similar to that observed in comet 67P/C-G as long as the density is high, the ionization rate is low, and the temperature is warm.

Here, we discuss the role of chemistry during protostellar collapse and protoplanetary disc formation on the observed abundance of O₂ in 67P/C-G. Material en route from the protostellar envelope into the disc is subject to increasing temperatures and UV radiation generated by the central (proto)star. We address the following two questions: (i) can O₂ gas and/or ice efficiently form during the formation of protostars and discs if the material composition is initially poor in molecular oxygen? and (ii) can O₂ ice coformed with H₂O ice in the pre-stellar stage be delivered to the comet-forming zone in young protoplanetary discs without significant chemical processing? To address those questions, the chemical evolution from pre-stellar cores to forming discs is calculated.

4.1 Model description

For the protostellar disc formation model, the axisymmetric semi-analytical two-dimensional model developed by Visser et al. (2009), Visser, Doty & van Dishoeck (2011) and adjusted by Harsono et al. (2013) is adopted. Briefly, the model describes the temporal evolution of the density and velocity fields following inside-out col-

lapse and the formation of an accretion disc described by the α-viscosity prescription (Shakura & Sunyaev 1973; Lynden-Bell & Pringle 1974; Shu 1977; Cassen & Moosman 1981; Terebey, Shu & Cassen 1984). Additional details can be found in the original papers. The vertical structure of the disc is calculated assuming hydrostatic equilibrium. The dust temperature and UV radiation field, which are critical for the chemistry, are calculated at each time step by solving the radiative transfer with RADMC-3D.[1] Outflow cavities are included by hand in a time-dependent manner (see Drozdovskaya et al. 2014, for details). Initially, the core has a power-law density distribution $\propto r^{-2}$, where r is the distance from the centre of the core, with an outer boundary of ~7000 au and a total mass of 1 M$_\odot$. Two values for the initial core rotation rate are investigated: $\Omega = 10^{-14}$ and 10^{-13} s^{-1}, corresponding to cases 3 and 7 in Visser et al. (2009), respectively. The model follows the physical evolution until the end of the main accretion phase when the gas accretion from the envelope on to the star–disc system is almost complete.

Fluid parcels from the envelope to the disc are traced in the physical model, and the Furuya astrochemical model is used to follow the gas–ice chemical evolution calculated along each individual trajectory with the parameters described in Section 2.5.

A molecular cloud formation model is run to determine the composition of the gas and ice in the parent molecular cloud (Furuya et al. 2015). The chemistry is then evolved for an additional 3×10^5 yr under pre-stellar core conditions to compute the abundances at the onset of collapse. The pre-stellar core density, temperature, and visual extinction are set to 4×10^4 cm^{-3}, 10 K, and 10 mag, respectively. At the onset of collapse, most oxygen ($\gtrsim 95$ per cent) is contained in icy molecules, e.g. H₂O and CO ice. The O₂ gas and ice abundances with respect to hydrogen nuclei are only 3×10^{-8} and $\ll 10^{-14}$, respectively, while the H₂O gas and ice abundances are 2×10^{-8} and 10^{-4}, respectively. Hence, the models using this set of initial abundances have a negligible O₂ ice abundance. Note that the O₂ gas abundance in both the molecular cloud formation stage and the pre-stellar core stage is lower than a few $\times 10^{-8}$, which is consistent with the upper limits of the observationally derived O₂ gas abundance towards nearby cold ($T \sim 10$ K) clouds (Goldsmith et al. 2000; Pagani et al. 2003; Furuya et al. 2015).

Following on from the preceding section, we also explore whether O₂ ice coformed with H₂O ice in the pre-stellar stage can be delivered to the comet-forming midplanes of protoplanetary discs without significant alteration. To do this, we also run models with an artificially increased initial O₂ ice abundance, set to be 5 per cent of that for H₂O ice.

4.2 Results

Fig. 8 shows the spatial distributions of fluid parcels at the final time of the simulation in models with $\Omega = 10^{-14}$ s^{-1} (infall dominated, top panels) and 10^{-13} s^{-1} (spread dominated, lower panels). For the case in which the ice mantle is poor in O₂ ice at the onset of collapse, it is found that (i) some gaseous O₂ can form (up to ~10^{-6}) depending on the trajectory paths (left-hand panels), and (ii) O₂ ice trapped within H₂O ice does not efficiently form en route into the disc (middle panels).

Given that most elemental oxygen is in ices (H₂O and CO) at the onset of collapse, gaseous O₂ forms through

---

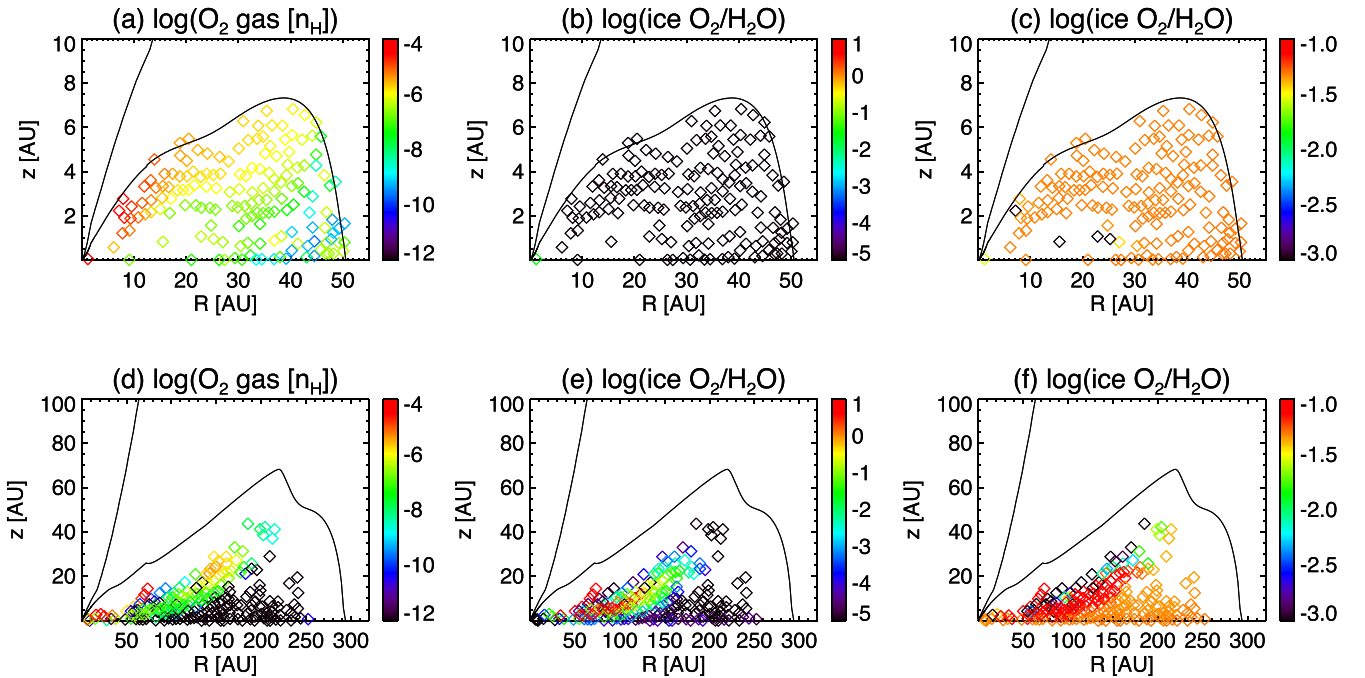[1] http://www.ita.uni-heidelberg.de/~dullemond/software/radmc-3d/

Figure 8. Spatial distributions of fluid parcels at the final time of the simulation. The top panels (a, b, c) represent the collapse model with $\Omega = 10^{-14}$ s^{-1}, while the bottom panels (d, e, f) represent the model with $\Omega = 10^{-13}$ s^{-1}. The left-hand panels (a, d) show the gaseous O_2 abundance with respect to hydrogen nuclei, while the middle panels (b, e) show the abundance ratio between O_2 ice and H_2O ice. The right-hand panels (c, f) also show the abundance ratio between O_2 ice and H_2O ice, but for those models where the initial ratio is artificially set to 5 per cent. The solid lines represent the outflow cavity wall and the disc surface.

photodissociation/desorption of H_2O ice by stellar UV photons in the warm (>20 K) protostellar envelope, followed by subsequent gas-phase reactions (e.g. O + OH). The middle panels of Fig. 8 show that the majority of parcels in each disc have a low final O_2/H_2O ice ratio, $\ll 10^{-2}$. However, the upper layers of the larger (i.e. higher Ω case) disc do have several parcels with a O_2/H_2O ice ratio higher than 10^{-2} (see panel e in Fig. 8). Analysis of the ice composition shows that the O_2 ice is associated with CO_2 ice rather than with H_2O. Upon water ice photodissociation, the warm temperatures encountered through the protostellar envelope mean that CO_2 ice (re)formation is more favourable than that for H_2O ice. This is due to the weak binding energy of atomic hydrogen: the reaction to form CO_2 ice (via e.g. CO + OH) proceeds faster than that for H_2O reformation (e.g. H + OH) as atomic hydrogen escapes back into the gas phase before it can diffuse and react with OH. Fig. 9 shows the correlation among the abundances of H_2O ice, O_2 ice, and CO_2 ice in the model with $\Omega = 10^{-13}$ s^{-1}. In regions where O_2 ice is relatively abundant (>1 per cent of H_2O ice), the CO_2 ice abundance is higher than or comparable to the H_2O ice abundance. Hence, these results show that it is difficult to form O_2 ice which is closely associated with H_2O ice during the process of core collapse and disc formation.

For the case that the simulations begin with an appreciable fraction of O_2 ice (5 per cent relative to water ice), the O_2/H_2O ratio throughout both discs is largely preserved. This is indicated by the relatively homogenous distribution of orange points in panels (c) and (f) in Fig. 8. Hence, O_2 which has a pre-stellar or molecular cloud origin is able to survive the chemical processing en route into the comet-forming regions of protoplanetary discs. Trajectories which are an exception to this rule are those which have been most exposed to stellar radiation; however, these trajectories are predominantly in the upper and closer-in layers of each protoplan-

etary disc and likely do not contribute to the composition of the comet-building material. This is consistent with the earlier finding by Visser et al. (2011) that most water ice is delivered to protoplanetary discs without alteration or sublimation.

5 O_2 FORMATION AND TRAPPING IN DISCS INDUCED BY LUMINOSITY OUTBURSTS?

5.1 Motivation

The simulations in the previous section show that O_2 can be produced in the gas phase in the intermediate layers of relatively warm forming discs (see panel a in Fig. 8), with an abundance a few per cent that of water ice (i.e. a fractional abundance of $\sim 10^{-6}$ with
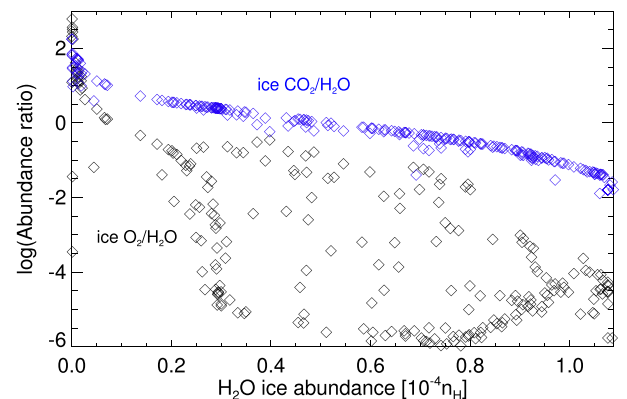

Figure 9. O_2 ice (black) and CO_2 ice (blue) abundances relative to H_2O as a function of H_2O ice abundance at the final time of the simulation in the model with $\Omega = 10^{-13}$ s^{-1} and the very low initial O_2 ice abundance.
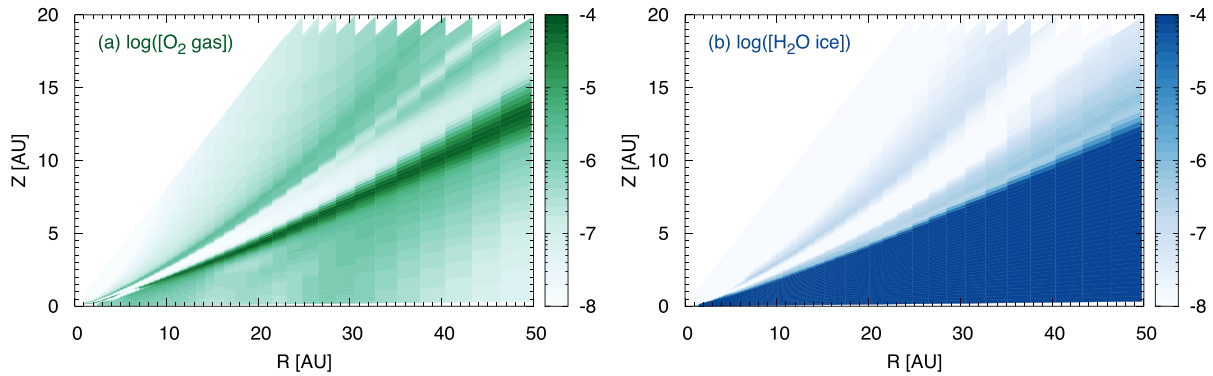
Figure 10. Fractional abundance (relative to H_2) of O_2 gas (left) and H_2O ice (right) as a function of disc radius and height, for a protoplanetary disc around a T Tauri star (data from Walsh et al. 2014).

respect to n_H). The origin of the gas-phase O_2 is driven by photo-processing of water ice by stellar UV photons en route into the disc, which releases photofragments required for forming O_2 (O and OH) into the gas phase. Relatively high abundances of gas-phase O_2 are also predicted in the inner regions of protoplanetary discs around already formed stars (e.g. Walsh et al. 2014, 2015). The origin of gas-phase O_2 in these models is similar to that in forming discs, except that the release of photofragments of water ice photodissoci-ation occurs over the lifetime of the disc ($\gtrsim 10^6$ yr) and is driven by the UV photons generated near the disc midplane by the interaction of cosmic rays with H_2. O_2 persists in the gas phase near the disc midplane because its volatility is such that it cannot freeze-out at the midplane temperatures within a few 10s of au (typically >20 K).

Fig. 10 shows the fractional abundance of O_2 gas (left) and H_2O ice (right) as a function of disc radius and height for a protoplanetary disc around a T Tauri star (data from Walsh et al. 2014). Similar abundances are seen for discs around both cooler (i.e. M dwarf) and hotter (i.e. Herbig Ae) stars, except that the water snowline is shifted to smaller and larger radii, respectively (see Walsh et al. 2015). The results show that O_2 gas can reach an abundance a few per cent of that of water ice in the comet formation zone ($\lesssim 50$ au).

The main issue with this scenario is whether a mechanism exists whereby gas-phase O_2 formed near the disc midplane, in either forming discs or more evolved discs, can become entrapped within, and thus associated with, the water-rich ice mantle, as seen in comet 67P/C-G. Observational and theoretical studies suggest that the luminosity evolution of low-mass stars is highly variable, with frequent and strong eruptive bursts, followed by long periods of relative quiescence (e.g. Herbig 1977; Hartmann & Kenyon 1985; Vorobyov & Basu 2005). Such luminosity outbursts could have a strong impact on the morphology and the chemical composition of ices near the protoplanetary disc midplane. The sudden temperature variations induced by short luminosity outbursts could gradually recycle the content of ices into the gas phase and modify their chemical structure via rapid and efficient freeze-out. If the luminosity outburst is sufficiently strong, warm gas-phase formation of molecular oxygen could be triggered by the evaporation of water ice, if the peak temperature during the outburst is higher than ~ 100 K. O_2 might then be recondensed together with water post outburst, if the cooling time-scale is shorter than the freeze-out time-scale, i.e. $\tau_{cool} < \tau_{fr}$, and also if the temperature reached after post-outburst is lower than the condensation temperature of O_2 (≈ 20 K).

An increase in temperature from ≈ 20 to ≈ 100 K during an outburst, corresponds roughly to an increase in luminosity by a factor

of ~ 600 assuming that the temperature in the disc and the central luminosity are linked through Stefan–Boltzmann's law. The recent hydrodynamical model by Vorobyov & Basu (2015) shows that a dozen of such strong luminosity outbursts, with typical durations of 10–100 yr, may occur during the disc lifetime. The exact number depends on the physical properties of the collapsing core and the disc.

5.2 Model description

The scenario of formation and recondensation of O_2 induced by a series of outburst events in discs is investigated by a series of outbursts occurring every 10^4 yr for a total time-scale of 10^5 yr. The astrochemical model and chemical network used are described in Section 2.5, while the assumed physical conditions are for a single point, motivated by protoplanetary disc models. Initial ice abundances are the median values derived by Öberg et al. (2011) from interstellar ice observations towards low-mass protostars. Thus it is assumed that the ice mantles are initially poor in O_2. The pre-outburst and post-outburst temperature is set to 20 K, corresponding approximately to the freeze-out temperature of O_2. Protoplanetary disc models suggest that the corresponding midplane density at this point is $\sim 10^8$ cm^{-3} (e.g. Furuya et al. 2013; Walsh et al. 2014); however, the exact relation between the dust temperature and gas density near protoplanetary disc midplanes depends on numerous factors including disc surface density (or mass), stellar spectral type, and the dust properties.

Gas-phase formation of O_2 is triggered by the photodissociation of water into H and OH and consequently is highly dependent on the assumed cosmic ray ionization rate, ζ, which is thought to be impeded near the disc midplane with respect to interstellar values (e.g. Cleeves et al. 2013). The impact of ζ on the formation of O_2 is investigated by considering two values which cover the possible range, $\zeta = 1 \times 10^{-18}$ and 1×10^{-17} s^{-1}.

The freeze-out time-scale of a neutral species i on to grains is given by

$$\tau_{fr} = 1.6 \times 10^2 \text{ yr} \frac{10^8 \text{ cm}^{-3}}{n_H} \frac{10^{-2}}{R_{dg}}$$

$$\times \frac{\rho_d}{3 \text{ g/cm}^3} \frac{a_d}{1 \text{ μm}} \sqrt{\frac{10 \text{ K}}{T}} \sqrt{M_i}, \tag{5}$$

where R_{dg} is the dust-to-gas mass ratio, ρ_d the volumic mass of grains, a_d the mean grain diameter, and M_i the weight of species i. Grain growth is expected to occur near protoplanetary disc

midplanes. Vasyunin et al. (2011) predict an average size of 1 μm with a dust-to-gas mass ratio of 0.01 in the midplane but the average size sharply decreases with altitude. Therefore, two grain sizes are considered $a_d = 0.1$ and 1 μm. For a fixed dust-to-gas mass ratio, R_{dg}, a larger grain size will increase the freeze-out time-scale, τ_{fr}, relative to the cooling time-scale, τ_{cool}, due to the reduction in total available dust-grain surface area. On the other hand, an increase in R_{dg}, perhaps due to settling and/or radial drift, will increase the total available grain surface area and will reduce the freeze-out time-scale.

Six models are run to investigate the impact of various parameters on the formation and the recondensation of O₂ during outbursts which last a time-scale, τ.

(i) Standard model with $a_d = 1$ μm, $\zeta = 1 \times 10^{-18}$ s⁻¹, $\tau = 100$ yr, $T_{max} = 100$ K.
(ii) Same as (i) but with $a_d = 0.1$ μm.
(iii) Same as (i) but with $\zeta = 1 \times 10^{-17}$ s⁻¹.
(iv) Same as (i) but with $\tau = 10$ yr.
(v) Same as (i) but with $T_{max} = 150$ K.
(vi) Same as (i) but with an initial O₂ abundance of 5 per cent relative to water.

Model (vi) is included to test the hypothesis that primordial O₂, formed during the molecular cloud stage, survives both transport into the forming protoplanetary disc and luminosity outbursts in the disc midplane. For the standard set of parameters [i.e. model (i)], the freeze-out time-scale following a burst is 100–200 yr (see equation 5). This is likely longer than the cooling time-scale (from ≈100 to 20 K), expected to be shorter than the duration of the outburst (<100 yr; Vorobyov & Basu 2015).

5.3 Results

Fig. 11 shows the fractional composition of ices in each monolayer as a function of monolayer, for the six models described above. Each line represents the abundance of each species prior to the next outburst (i.e. following each period of cooling and quiescence). In general, regardless of the assumed physical parameters, the volatile component of the ice mantle increases with time. The ice profile is composed of two main parts: (i) a volatile-free deeper ice mantle mostly composed of water ice and other non-volatile species, such as CH₃OH, that primarily remain on grains during the outbursts because the temperature reached during the outburst is only slightly higher than their evaporation temperature, and (ii) an upper ice mantle composed of water ice, but also of volatile species, such as CO, O₂, and N₂, that freeze-out during the post-outburst cooling. The deeper and volatile-free ice mantle increases in mass/depth with the duration of the outburst (compare panels a and d in Fig. 11) and with decreasing grain size that increases the surface area of dust (compare panels a and b in Fig. 11).

The fraction of O₂ trapped in the ice mantle increases with the outburst duration, the grain size, and the cosmic ray ionization rate, ζ, all parameters which favour the formation of gaseous O₂ from water during the outburst. Increasing the grain size decreases the total grain cross-sectional area and therefore the accretion rate of gas-phase species on to the ice mantle, allowing water and other species to spend more time in the gas phase for reaction. A higher ζ increases the production of OH from the photodissociation of water vapour, necessary to form O₂. Allowing the peak temperature during outburst to reach values higher than the evaporation temperature of water ice ($T_{max} = 150$ K, panel e in Fig. 11), results in full sublimation of the ice mantle prior to recondensation. How-

ever, the enhanced abundance of water released into the gas phase does not significantly enhance the abundance of O₂ formed, and subsequently trapped. in the ice mantle. The luminosity outburst period and duration considered here are potentially too short and also too infrequent to reproduce the high amount of O₂ observed in 67P/C-G. Maximum O₂ abundances of a few × 0.1 per cent only are predicted.

Results for the calculation with 5 per cent of O₂ (relative to water ice) already present in the ice show that O₂ can survive and be efficiently trapped within the water-rich ice mantle following a series of luminosity outbursts. Hence, O₂ may become associated with water ice in the disc midplane via release and recondensation driven by outbursts. However, other volatile species such as CO and N₂ are also trapped within the water ice, which is in contradiction with the observations towards 67P/C-G. CO and N₂ are shown to be depleted in 67P/C-G relative to interstellar values, and the molecules are not strongly correlated with water in the comet coma, converse to the case for O₂ (Bieler et al. 2015; Rubin et al. 2015a). Note also that interstellar ices produced after luminosity outbursts are likely amorphous in structure (Kouchi et al. 1994).

6 SUMMARY

In this work, sophisticated astrochemical models are used to investigate the chemical and physical origin of molecular oxygen in comet 67P/C-G as observed with *Rosetta*/ROSINA. The observations show that molecular oxygen is not only strongly associated with water, but is also the fourth most abundant molecule in the coma, at ∼4 per cent of the water abundance (Bieler et al. 2015).

We tested the formation and survival of O₂ (and related species) in models covering a range of dark cloud physical conditions (temperature, density, and cosmic ray ionization rate). We found that the efficiency of the formation of molecular oxygen increases for higher densities ($\gtrsim 10^5$ cm⁻³), moderate temperatures (≈20 K), and moderate ionization rates ($\lesssim 10^{-16}$ s⁻¹). These conditions lower the ratio of H/O in the gas phase, thereby impeding the conversion of O₂ ice into H₂O ice. These parameters are found to be in good agreement with the physical conditions for the dark cloud ρ Oph A, one of the two interstellar regions where O₂ has been detected. The high O₂ abundances do not require photolysis of bulk ice as the main process but are the result of surface reactions building up the ice layers.

We next tested whether molecular oxygen can be efficiently formed in the ice mantle during protostellar disc formation. For models in which the initial ice composition is assumed to be poor in O₂, O₂ can produced only through gas-phase chemistry induced by processing of the water-rich ice mantle by stellar UV radiation in the intermediate layers of the protoplanetary disc, with abundance levels similar to that in 67P/C-G but ices in the disc midplane remain poor in O₂. For models in which the ice mantles were originally abundant in molecular oxygen (≈5 per cent relative to water), for both disc models, we find that the oxygen is delivered to the comet-forming zone without sublimation nor alteration. Hence, if molecular oxygen has a primordial origin as suggested by the dark cloud models, then it can survive transport into the protoplanetary disc.

Given that gas-phase O₂ can form near protoplanetary disc midplanes, and reach abundances relative to water ice similar to that in 67P/C-G, we finally tested whether luminosity outbursts which increase the local temperature to >100 K, aid the formation and entrapment of gas-phase O₂ into the water-rich ice mantle. Although laboratory experiments show that O₂ can be efficiently formed
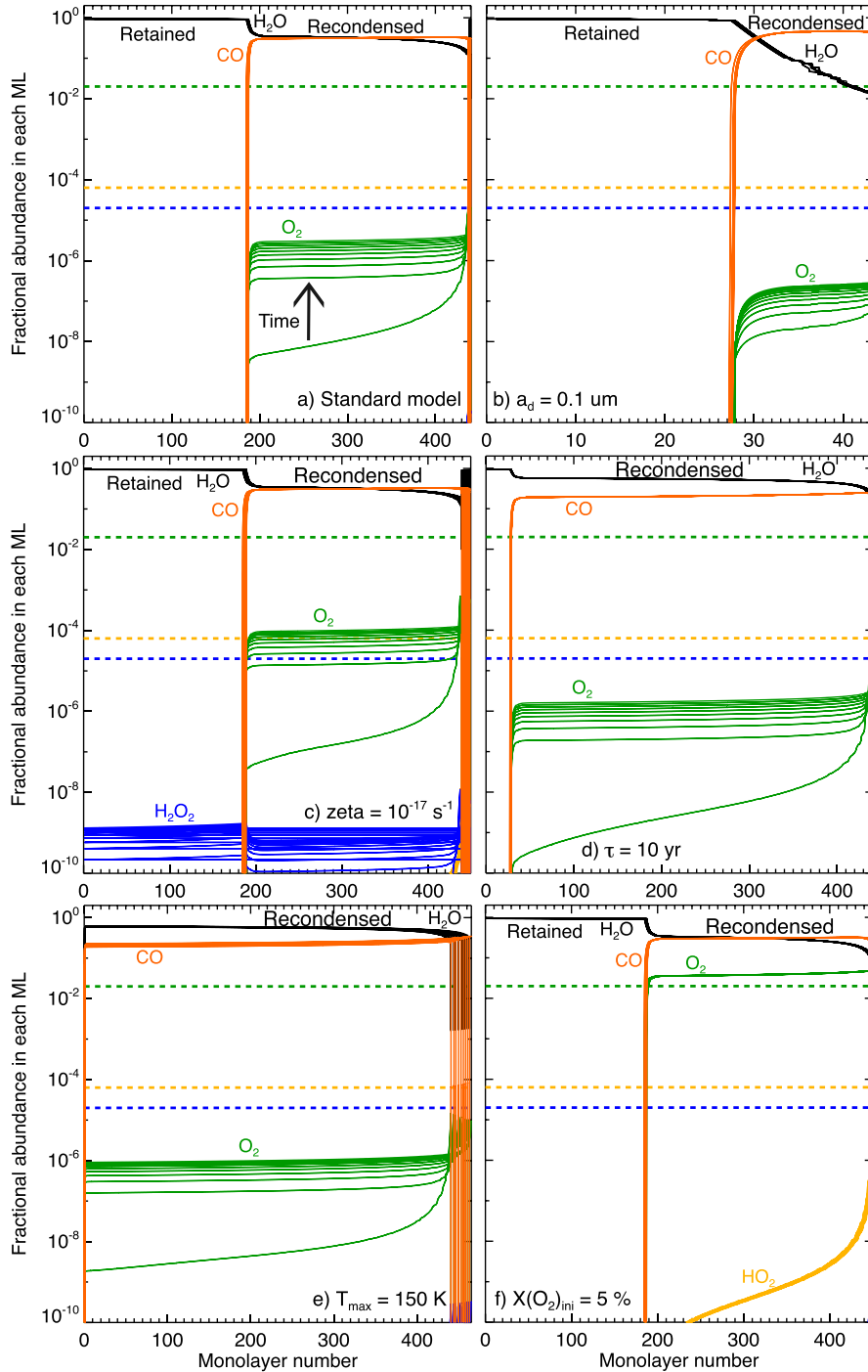
Figure 11. Fractional composition of each monolayer within ices during the 10 luminosity outbursts for the six models considered in this work (see the text for more details). The standard parameters are $a_d = 1$ μm, $\zeta = 1 \times 10^{-18}$ s^{-1}, $\tau = 100$ yr, $T_{max} = 100$ K. The thick dashed lines refer to the abundances observed in the comet 67P/C-G.

within water ices during the ice recondensation through radiolysis (Teolis et al. 2006), we consider this less likely because the cosmic ray ionization rate and energetic particles from the (pre)solar wind are expected to be significantly attenuated near the disc midplane. It is found that the maximum amount of O_2 formed during luminosity outbursts and then trapped within the ice mantle during the cooling depends on several parameters, such as grain size, ionization rate, or the outburst duration, but never exceeds ~0.1 per cent. Assuming an initial O_2 abundance of 5 per cent relative to water ice results

in an efficient trapping of O_2 within the water–ice mantle due to the fast cooling after the outburst. However, in that case also other volatile species, such as CO and N_2, become trapped, which is in contradiction with observations towards 67P/C-G.

In summary, the models presented here favour the scenario that molecular oxygen in 67P/C-G has a primordial origin (i.e. formed in the molecular cloud) and has survived transport through the protostellar envelope and into the comet-forming regions of protoplanetary discs. The 'primordial' origin of O_2 is in good agreement with

the conclusions of Mousis et al. (2016). However, while Mousis et al. (2016) invoked radiolysis to efficiently convert water ice to O_2, we find that the entrapment and strong association with water ice combined with low abundance of species like H_2O_2, HO_2, or O_3 can alternatively be explained by an efficient O_2 formation at the surface of interstellar ices through oxygen atom recombination in relatively warmer ($\sim$20 K) and denser ($n_H \gtrsim 10^5$ cm^{-3}) conditions than usually expected in dark clouds. The weak correlation of CO and N_2 with water seen in 67P/C-G is explained by a later formation of these species in dark clouds with respect to O_2 and water. This picture would therefore be consistent with the physical and chemical properties of our Solar system, such as the presence of short-lived radio isotopes in meteorites or the orbits of Solar system planets, suggesting that our Solar system was born in a dense cluster of stars (see Adams 2010).

ACKNOWLEDGEMENTS

REFERENCES

Acharyya K., Fuchs G. W., Fraser H. J., van Dishoeck E. F., Linnartz H., 2007, A&A, 466, 1005
Adams F. C., 2010, ARA&A, 48, 47
Altwegg K. et al., 2015, Science, 347, 1261952
Andersson S., van Dishoeck E. F., 2008, A&A, 491, 907
Andersson S., Al-Halabi A., Kroes G. J., van Dishoeck E. F., 2006, J. Chem. Phys., 124, 4715
Arasa C., Koning J., Kroes G.-J., Walsh C., van Dishoeck E. F., 2015, A&A, 575, A121
Atkinson R. et al., 2004, Atmos. Chem. Phys., 4, 1461
Balsiger H. et al., 2007, Space Sci. Rev., 128, 745
Baragiola R. A., Atteberry C. L., Dukes C. A., Famá M., Teolis B. D., 2002, Nucl. Instrum. Methods Phys. Res. B, 193, 720
Bergeron H., Rougeau N., Sidis V., Sizun M., Teillet-Billy D., Aquillon F., 2008, J. Phys. Chem. A, 112, 11921
Bergman P., Parise B., Liseau R., Larsson B., 2011a, A&A, 527, A39
Bergman P., Parise B., Liseau R., Larsson B., Olofsson H., Menten K. M., Güsten R., 2011b, A&A, 531, L8
Bieler A. et al., 2015, Nature, 526, 678
Cassen P., Moosman A., 1981, Icarus, 48, 353
Cazaux S., Minissale M., Dulieu F., Hocuk S., 2016, A&A, 585, A55
Chen, J.-H. et al., 2014, ApJ, 793, 111
Cleeves L. I., Adams F. C., Bergin E. A., 2013, ApJ, 772, 5
Cleeves L. I., Bergin E. A., Alexander C. M. O., Du F., Graninger D., Öberg K. I., Harries T. J., 2014, Science, 345, 1590
Collings M. P., Dever J. W., Fraser H. J., McCoustra M. R. S., Williams D. A., 2003, ApJ, 583, 1058
Collings M. P., Anderson M. A., Chen R., Dever J. W., Viti S., Williams D. A., McCoustra M. R. S., 2004, MNRAS, 354, 1133
Collings M. P., Frankland V. L., Lasne J., Marchione D., Rosu-Finsen A., McCoustra M. R. S., 2015, MNRAS, 449, 1826
Cuppen H. M., Herbst E., 2007, ApJ, 668, 294
Cuppen H. M., Ioppolo S., Romanzin C., Linnartz H., 2010, Phys. Chem. Chem. Phys., 12, 12077
Drozdovskaya M. N., Walsh C., Visser R., Harsono D., van Dishoeck E. F., 2014, MNRAS, 445, 913
Du F., Parise B., 2012, A&A, 538, A91
Du F., Parise B., Bergman P., 2012, A&A, 541, L11
Dulieu F., 2011, in Cernicharo J., Bachiller R., eds, Proc. IAU Symp. 280, The Molecular Universe. Cambridge Univ. Press, Cambridge, p. 405
Fayolle E. C. et al., 2013, A&A, 556, A122
Fuchs G. et al., 2006, Faraday Discussions, 133, 331
Furuya K., Aikawa Y., Nomura H., Hersant F., Wakelam V., 2013, ApJ, 779, 11
Furuya K., Aikawa Y., Hincelin U., Hassel G., Bergin E. A., Vasyunin A. I., Herbst E., 2015, A&A, 584, A124
Furuya K. et al., 2016, A&A, in press
Garrod R. T., Herbst E., 2006, A&A, 457, 927
Garrod R. T., Wakelam V., Herbst E., 2007, A&A, 467, 1103
Garrod R. T., Weaver S. L. W., Herbst E., 2008, ApJ, 682, 283
Goldsmith P. F. et al., 2000, ApJ, 539, L123
Goldsmith P. F. et al., 2011, ApJ, 737, 96
Hall D. T., Strobel. D. F., Feldman P. D., McGrath M. A., Weaver H. A., 1995, Nature, 373, 677
Hand K. P., Carlson R. W., 2011, Icarus, 215, 226
Harada N., Herbst R., Wakelam V., 2010, ApJ, 721, 1570
Harsono D., Visser R., Bruderer S., van Dishoeck E. F., Kristensen L. E., 2013, A&A, 555, A45
Hartmann L., Kenyon S. J., 1985, ApJ, 299, 462
Hasegawa T. I., Herbst E., 1993, MNRAS, 263, 589
He J., Shi J., Hopkins T., Vidali G., Kaufman M. J., 2015, ApJ, 801, 120
Heays A. N., Bosman A. D., van Dishoeck E. F., 2016, ApJS, in press
Herbig G. H., 1977, ApJ, 217, 693
Hincelin U., Wakelam V., Hersant F., Guilloteau S., Loison J. C., Honvault P., Troe J., 2011, A&A, 530, A61
Ioppolo S., Cuppen H. M., Romanzin C., van Dishoeck E. F., Linnartz H., 2008, ApJ, 686, 1474
Ioppolo S., Cuppen H. M., Romanzin C., van Dishoeck E. F., Linnartz H., 2010, Phys. Chem. Chem. Phys., 12, 12065
Jaycock M. J., Parfitt G. D., 1986, Chemistry of Interfaces. Wiley, New York
Karssemeijer L. J., Cuppen H. M., 2014, A&A, 569, A107
Katz N., Furman I., Biham O., Pirronello V., Vidali G., 1999, ApJ, 522, 305
Kouchi A., Yamamoto T., Kozasa T., Kuroda T., Greenberg J. M., 1994, A&A, 290, 1009
Lamberts T., Cuppen H. M., Ioppolo S., Linnartz H., 2013, Phys. Chem. Chem. Phys., 15, 8287
Larsson B. et al., 2007, A&A, 466, 999
Liseau R., Larsson B., Bergman P., Pagani L., Black J. H., Hjalmarson Å., Justtanont K., 2010, A&A, 510, A98
Liseau R. et al., 2012, A&A, 541, A73
Loeffler M. J., Raut U., Vidal R. A., Baragiola R. A., Carlson R. W., 2006, Icarus, 180, 265
Lynden-Bell D., Pringle J. E., 1974, MNRAS, 168, 603
McElroy D., Walsh C., Markwick A. J., Cordiner M. A., Smith K., Millar T. J., 2013, A&A, 550, A36
Matar E., Congiu E., Dulieu F., Momeni A., Lemaire J. L., 2008, A&A, 492, L17
Matich A. J., Bakker M. G., Lennon D., Quickenden T. I., Freeman C. G., 1993, J. Phys. Chem., 97, 10539
Melius C. F., Blint R. J., 1979, Chem. Phys. Lett., 64, 183
Melnick G. J., Kaufman M. J., 2015, ApJ, 806, 227
Minissale M., Dulieu F., 2014, J. Chem. Phys., 141, 014304
Minissale M., Congiu E., Dulieu F., 2014, J. Chem. Phys., 140, 074705
Minissale M., Dulieu F., Cazaux S., Hocuk S., 2016, A&A, 585, A24
Miyauchi N., Hidaka H., Chigai T., Nagaoka A., Watanabe N., Kouchi A., 2008, Chem. Phys. Lett., 456, 27
Mousis O. et al., 2016, ApJ, 823, L41
Noble J., Congiu E., Dulieu F., Fraser H. J., 2012, MNRAS, 421, 768
Öberg K. I., Linnartz H., Visser R., van Dishoeck E. F., 2009, ApJ, 693, 1209

Öberg K. I., Boogert A. C. A., Pontopiddan K. M., van den Broek S., van Dishoeck E. F., Bottinelli S., Blake G. A., Evans N. J., II, 2011, ApJ, 740, 109

Pagani L. et al., 2003, A&A, 402, L77

Perets H. B., Biham O., Manicó G., Pirronello V., Roser J., Swords S., Vidali G., 2005, ApJ, 627, 850

Pontoppidan K. M. et al., 2003, A&A, 408, 981

Prasad S. S., Tarafdar S. P., 1983, ApJ, 267, 603

Rimola A., Taquet V., Ugliengo P., 2014, A&A, 572, A70

Rubin M. et al., 2015a, Science, 348, 232

Rubin M., Altwegg K., van Dishoeck E. F., Schwehm G., 2015b, ApJ, 815, L11

Shakura N. I., Sunyaev R. A., 1973, A&A, 24, 337

Shu F. H., 1977, ApJ, 214, 488

Sieger M. T., Simpson W. C., Orlando T. M., 1998, Nature, 394, 554

Snellen I. A. G., de Kok R. J., le Poole R., Brogi M., Birkby J., 2013, ApJ, 764, 182

Spencer J. R., Calvin W. M., Person M. J., 1995, J. Geophys. Res., 100, 19049

Taquet V., Ceccarelli C., Kahane C., 2012, A&A, 538, A42

Taquet V., Peters P., Kahane C., Ceccarelli C., López-Sepulcre A., Toubin C., Duflot D., Wiesenfeld L., 2013, A&A, 550, A127

Taquet V., Charnley S. B., Sipilä O., 2014, ApJ, 791, 1

Teolis B. D., Loeffler M. J., Raut U., Famá M., Baragiola R. A., 2006, ApJ, 644, L141

Teolis B. D. et al., 2010, Science, 330, 1813

Terebey S., Shu F. H., Cassen P., 1984, ApJ, 286, 529

Tielens A. G. G. M., 2005, The Physics and Chemistry of the Interstellar Medium. Cambridge Univ. Press, Cambridge

Tielens A. G. G. M., 2013, Rev. Modern Phys., 85, 1021

Tielens A. G. G. M., Allamandola L. J., 1987, in Hollenbach D. J., Thronson H. A., eds, Interstellar Processes. Reidel, Dordrecht, p. 397

Tielens A. G. G. M., Hagen W., 1982, A&A, 114, 245

Vandenbussche B. et al., 1999, A&A, 346, L57

van Dishoeck E. F., Herbst E., Neufeld D. A., 2013, Chem. Rev., 113, 9043

Vasyunin A. I., Herbst E., 2013, ApJ, 762, 86

Vasyunin A. I., Wiebe D. S., Birnstiel T., Zhukovska S., Henning T., Dullemond C. P., 2011, ApJ, 727, 76

Visser R., van Dishoeck E. F., Doty S. D., Dullemond C. P., 2009, A&A, 495, 881

Visser R., Doty S. D., van Dishoeck E. F., 2011, A&A, 534, A132

Vorobyov E. I., Basu S., 2005, ApJ, 633, L137

Vorobyov E. I., Basu S., 2015, ApJ, 805, 115

Wakelam V., Herbst E., 2008, ApJ, 680, 371

Wakelam V. et al., 2012, ApJS, 199, 21

Walch S., Duchovic R., 1991, J. Chem. Phys., 94, 706

Walsh C., Millar T. J., Nomura H., Herbst E., Widicus Weaver S., Aikawa Y., Laas J. C., Vasyunin A. I., 2014, A&A, 563, A33

Walsh C., Nomura H., van Dishoeck E. F., 2015, A&A, 582, A88

Westley M. S., Baragiola R. A., Johnson R. E., Baratta G. A., 1995, Nature, 373, 405

Yildiz U. A. et al., 2013, A&A, 558, A58

Zhen J., Linnartz H., 2014, MNRAS, 437, 3190

Zheng W., Jewitt D., Kaiser R. I., 2006, ApJ, 639, 534

APPENDIX A: IMPACT OF CHEMICAL PARAMETERS ON THE COMPOSITION OF INTERSTELLAR ICES

A set of models is run, in order to investigate the impact of various surface and chemical parameters on the chemical composition of interstellar ices and to assess whether the abundances of O_2, O_3, HO_2, and H_2O_2 observed in comet 67P/C-G can be reproduced simultaneously. In each model, the 'standard' values of the input parameters, listed in Table 2, are assumed and only one of the parameters is varied in turn. In particular, the physical conditions
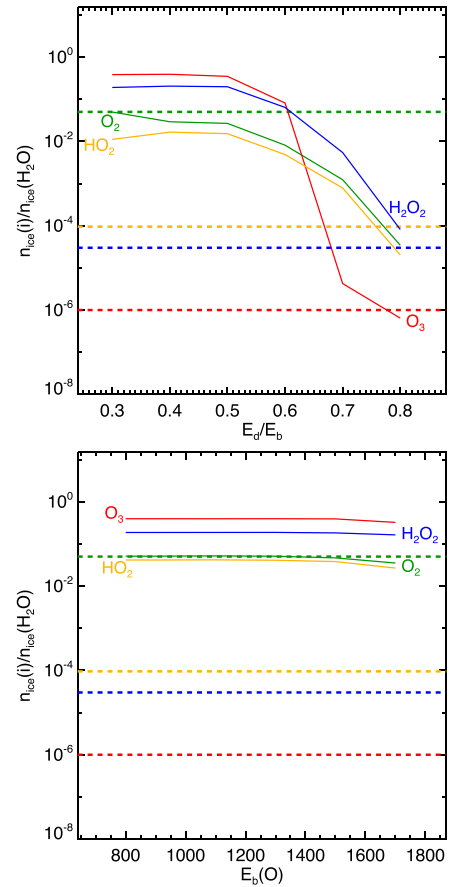

Figure A1. Abundances of O_2, O_3, HO_2, and H_2O_2 in interstellar ices (with respect to water ice) at a time of 4.4×10^4 yr, when the gas-phase O_2 abundance of the standard model reaches the abundance observed in ρ Oph A, for different values of the surface parameters E_d/E_b (left) and $E_b(O)$ (right). The thick dashed lines refer to the abundances observed in the comet 67P/C-G.

assumed here are conditions that favour a high production of O_2, i.e. a high density $n_H = 1 \times 10^6$ cm^{-3} and a warm temperature $T = 20$ K, according to the discussion in Section 2.4.

The impact of two surface parameters, the diffusion-to-binding energy ratio, E_d/E_b, and the binding energy for O on the formation and survival of O_2 ice and the chemically related species is investigated first. Following the discussion in Section 2.4, models in which the diffusion-to-binding energy ratio ranges between 0.3 and 0.8 and for which the binding energy of atomic oxygen ranges between 800 and 1700 K have been run. Fig. A1 shows the abundances of O_2, O_3, HO_2, and H_2O_2 in the solid phase (relative to water ice), at a time of 4.4×10^4 yr for the different values of the input chemical parameters. The abundance of O_2 (and that for chemically related species) tends to decrease as E_d/E_b is increased, both in the gas phase and in the ice mantle. The formation rate of O_2 is governed by the mobility of O atoms. Because of their relatively high binding energy (1700 K for the standard model), O atoms can diffuse efficiently only if $E_d/E_b \lesssim 0.6$. Higher values strongly inhibit the mobility, leading to a low abundance of O_2, O_3, HO_2, and H_2O_2 (see top panel in Fig. A1). Decreasing the binding energy of O atoms from 1700 to 800 K increases their mobility but also increases the rate of evaporation at 20 K. This then limits the conversion from O to O_2 and O_3, leading to a negligible dependence of the final abundances upon the assumed binding energy for atomic oxygen
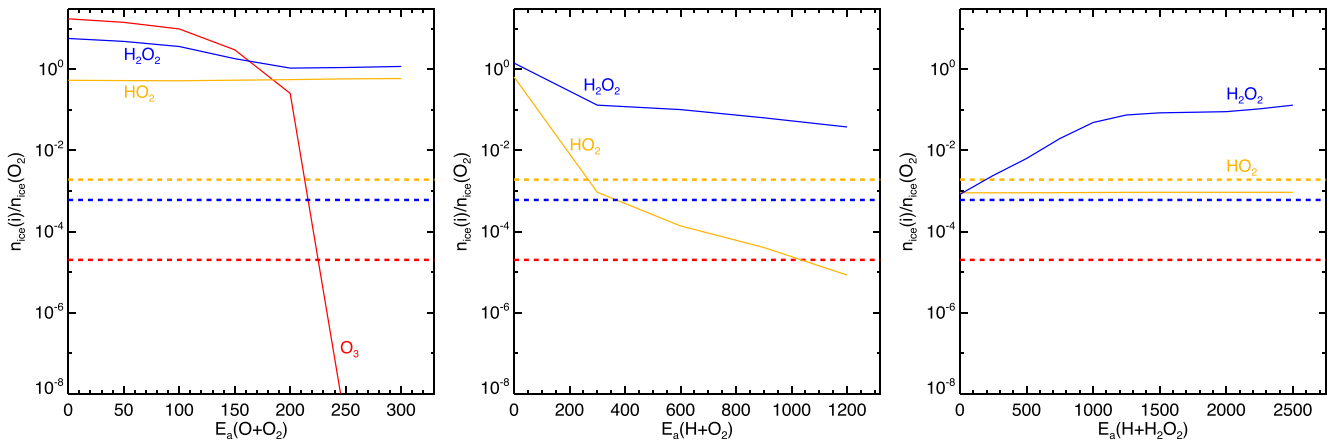
Figure A2. Abundances of O$_3$, HO$_2$, and H$_2$O$_2$ in interstellar ices (with respect to O$_2$) at a time of 4.4×10^4 yr for different values of the activation barriers of the reactions O + O$_2$ (left), H + O$_2$ (middle), and H + H$_2$O$_2$ (right). Models of the left-hand panels assume the standard values for the parameters listed in Table 2, while models of the middle panels assume an activation barrier for the reaction O + O$_2$ of 300 K, and models of the right-hand panels assume an activation barrier of 300 K for the reactions O + O$_2$ and H + O$_2$ (see text for more details). The thick dashed lines refer to the abundances observed in the comet 67P/C-G.

(see bottom panel in Fig. A1). The high abundance of O$_2$ seen in 67P/C-G can be reproduced for dense and warm conditions and assuming the standard values for the diffusion-to-binding energy ratio and the binding energy of atomic O. However, the abundances of O$_3$, HO$_2$, H$_2$O$_2$ are overproduced by more than two orders of magnitude when standard values for the activation barriers of surface reactions are assumed.

The impact of the activation barriers of the reactions O + O$_2$, H + O$_2$, and H + H$_2$O$_2$ on the abundances of O$_3$, HO$_2$, and H$_2$O$_2$ in ices is explored next. Fig. A2 shows how the abundances of O$_3$, HO$_2$, and H$_2$O$_2$ in the gas phase (top row) and in the solid phase (bottom row) relative to O$_2$ vary with the activation barriers of these three reactions. As described in Section 2.4, surface reactions involving O$_2$ have small or negligible reaction barriers but the activation barrier of the reaction O + O$_2$ remains uncertain. Because of the relatively high masses of O and O$_2$, the activation barrier can be only overcome thermally. At a dust temperature of 21 K, the reaction probability exponentially decreases from 1 ($E_a = 0$ K) to 6×10^{-7} ($E_a = 300$ K). As a consequence, a small activation barrier of 250–300 K favours the formation and survival of O$_2$, HO$_2$, and H$_2$O$_2$ with respect to O$_3$ and allows us to reproduce the low O$_3$/O$_2$ abundance ratio seen in comet 67P/C-G. This result is in good agreement with the results of Lamberts et al. (2013) who needed to introduce an activation barrier of 500 K in their microscopic Monte Carlo model to explain the slow formation of ozone observed in laboratory experiments of Ioppolo et al. (2010). The O + O$_2$ reaction still takes place and induces the evaporation of O$_3$ into the gas phase via chemical desorption, explaining the high abundance of O$_3$ in the gas phase. However, this occurs at a slower rate than the reactions destroying O$_3$ ice through barrierless surface reactions.

In the model results, a high abundance of O$_2$ ice is consistently accompanied by similar abundances of HO$_2$ and H$_2$O$_2$ ice, because the H + O$_2$ reaction is assumed to be barrierless, following the laboratory experiments of Miyauchi et al. (2008) and Ioppolo et al. (2008, 2010). However, quantum chemistry calculations by Walch & Duchovic (1991) show that the reaction in the gas phase has an activation barrier whose exact value depends on the incoming angle of the molecule. Lamberts et al. (2013) introduced a small activation

barrier of 200–400 K for this reaction in their Monte Carlo model to reproduce the chemical composition observed in cold ices produced in the laboratory experiments by Ioppolo et al. (2010). The activation barrier of the reaction H + O$_2$ was therefore varied between 0 (our standard value) and 1200 K, the energy computed for gas-phase conditions by Melius & Blint (1979). The transmission probability through quantum tunnelling was computed assuming a rectangular barrier with a standard width of 1 Å. As shown in the middle panel of Fig. A2, the abundance of HO$_2$ ice decreases sharply with the activation barrier of the reaction H + O$_2$, even for moderate values because its rate of formation becomes much lower than its rate of destruction while the decrease of the abundance of solid H$_2$O$_2$ is more limited. A small activation barrier of 300 K, similar to the values found by Lamberts et al. (2013), is therefore sufficient to reproduce the low abundance of HO$_2$ relative to O$_2$ observed in comet 67P/C-G.

The standard activation barrier of the H + H$_2$O$_2$ reaction of 2500 K and the associated transmission probability computed with the Eckart model follow the quantum chemical calculations for gas-phase conditions presented in Taquet et al. (2013). As for other reactions showing high activation barriers, the exact value of their barrier is highly uncertain and could be lowered in interstellar ices, due to the van der Waals interactions between the neighbouring water molecules and the reactants, as shown for instance by Rimola, Taquet & Ugliengo (2014) for the case of the CO + H and H$_2$CO + H reactions. Lamberts et al. (2013) decreased the activation barrier for the H + H$_2$O$_2$ to 800–1200 K in their Monte Carlo model to reproduce the H$_2$O$_2$ abundance in laboratory cold ices. The right-hand panel of Fig. A2 presents the evolution of the O$_3$, HO$_2$, and O$_3$ abundances relative to O$_2$ for different values of the activation barrier of the reaction H + H$_2$O$_2$, and assuming an activation barrier of 300 K for the reactions O + O$_2$ and H + O$_2$. The model tends to overpredict the abundance of H$_2$O$_2$ relative to the abundance observed in 67P/C-G, unless the reaction H + H$_2$O$_2$ is assumed to be effectively barrierless.

This paper has been typeset from a TEX/LATEX file prepared by the author.